Two charge states of the C_N acceptor in GaN: Evidence from photoluminescence

M. A. Reshchikov,[1,*] M. Vorobiov,[1] D. O. Demchenko,[1] Ü. Özgür,[2] H. Morkoç,[1,2] A. Lesnik,[3] M. P. Hoffmann,[3,†] F. Hörich,[3] A. Dadgar,[3] and A. Strittmatter[3]

[1]*Department of Physics, Virginia Commonwealth University, Richmond, Virginia 23284, USA*

[2]*Department of Electrical and Computing Engineering, Virginia Commonwealth University, Richmond, Virginia 23284, USA*

[3]*Institut für Physik, Otto-von-Guericke-Universität Magdeburg, Universitätsplatz 2, 39106 Magdeburg, Germany*

(Received 2 July 2018; published 28 September 2018)

We have found a photoluminescence (PL) band with unusual properties in GaN. The blue band, termed as the BL_C band, has a maximum at about 2.9 eV and an extremely short lifetime (shorter than 1 ns for a free-electron concentration of about 10^{18} cm^{-3}). The electron- and hole-capture coefficients for this defect-related band are estimated as 10^{-9} and 10^{-10} cm^3/s, respectively. The BL_C band is observed only in GaN samples with relatively high concentration of carbon impurity, where the yellow luminescence (the YL1 band) with a maximum at 2.2 eV is the dominant defect-related PL. Both the YL1 and BL_C bands likely originate from the C_N defect, namely, from electron transitions via the $-/0$ and $0/+$ thermodynamic transition levels of the C_N. The BL_C band appears only at high excitation intensities in *n*-type GaN samples codoped with Si and C, and it can be found in a wide range of excitation intensities in semi-insulating (presumably *p*-type) GaN samples doped with C. The properties and behavior of the YL1 and BL_C bands can be explained using phenomenological models and first-principles calculations.

DOI: 10.1103/PhysRevB.98.125207

I. INTRODUCTION

The yellow luminescence (YL) band with a maximum at about 2.2 eV is the dominant defect-related photoluminescence (PL) band in undoped and C-doped *n*-type GaN [1,2]. Contrary to widespread proposals that several defects can cause the YL band with similar spectral shape and position of maximum [3–5], we recently concluded that a single defect (the YL1 center) is responsible for the commonly observed YL bands in GaN, which sometimes vary in appearance and behavior [6,7]. The YL1 band has a maximum ($\hbar\omega_{max}$) at $\sim$2.20 eV and the zero-phonon line (ZPL or E_{01}) at 2.57 ± 0.01 eV for transitions from shallow donors to the YL1 center in the limit of low temperatures. The thermodynamic transition level (E_{A1}) for this defect is located at 0.916 ± 0.003 eV above the valence-band maximum. These and other fingerprints of the YL1 band (electron- and hole-capture coefficients, band position, and shape) allow a reliable recognition of this defect in the PL spectrum. We observed the YL1 band in a variety of GaN samples grown by different techniques, namely, in undoped, C-, Fe-, and Si-doped GaN grown by metalorganic vapor phase epitaxy (MOVPE), undoped GaN grown by hydride vapor phase epitaxy (HVPE), and undoped GaN grown by molecular beam epitaxy (MBE). The identity of the defect responsible for the YL1 band remained uncertain for decades, and only now has a sufficient amount of experimental and theoretical evidence been garnered to resolve this long-standing puzzle.

According to early first-principles calculations, based on the density functional theory (DFT) in the local-density approximation, the gallium vacancy (V_{Ga})-related defects, such as V_{Ga} or $V_{Ga}O_N$ [8,9], were considered to be the best candidates for the YL-related acceptor in undoped GaN [10]. The attribution of the YL band to the V_{Ga} or $V_{Ga}O_N$ became widely accepted [1] after Saarinen *et al.* [11] reported a correlation between the YL intensity and the concentration of the V_{Ga}-related defects obtained from positron annihilation experiments. In Sec. IV C, we provide the evidence that the V_{Ga}-related defects do not contribute to the commonly observed YL band.

Meanwhile, numerous experiments indicate that carbon is involved in the YL-related defect [1,2,3,12]. The idea that an isolated carbon (C_N) is the responsible defect was initially rejected by theorists because the DFT calculations predicted that the C_N is a shallow acceptor [8]. However, recent first-principles calculations, which employed a more sophisticated hybrid density functional theory [13], indicate that the C_N is in fact a deep acceptor with the $-/0$ transition level at 0.9 eV, in excellent agreement with the YL band parameters [14].

One remaining problem is that, according to the calculations, the C_N defect is also expected to have another transition level: the $0/+$ level at about 0.4 eV above the valence-band maximum [15,16]. Recombination of an electron from the conduction band (or from shallow donors at low temperatures) with a hole at the $0/+$ level of the C_N is expected to cause a PL band in the green or blue region of the PL spectrum [15,16]. In particular, for *n*-type GaN, transitions via the $0/+$ level may become noticeable at high excitation intensities after the C_N acceptors are saturated with photogenerated holes, which would then pave the way for them to capture a second hole to become C_N^+. At low excitation intensities (before

*mreshchi@vcu.edu

†Present address: Osram Opto Semiconductors, Regensburg, Germany.

the "primary" YL1 band is saturated), the intensity of this "secondary" PL band is expected to increase quadratically with the excitation intensity.

A green luminescence band (GL1) with a maximum at 2.40 eV was previously suggested to be a promising candidate for the secondary band due to its near-quadratic excitation intensity dependence [17,18]. However, after careful analyses of a large number of GaN samples we found no consistent correlation between the YL1 and GL1 bands. Moreover, the YL1 band is typically very strong in MOVPE-grown GaN contaminated with C due to growth conditions, and these samples never reveal the GL1 band. In contrast, the GL1 band is observed in HVPE-grown GaN in which the concentration of C is typically very low.

The quest for the source of the secondary PL band for the C_N acceptor has so far been unsuccessful. Although Lyons *et al.* [16] proposed that the blue luminescence band observed in C-doped GaN [19,20] is due to electron transitions from the conduction band to the C_N^+ defect, we show in Secs. III F and IV C that the blue band observed in those experiments has a different origin. One should note that several types of defects could cause similar PL bands; therefore, careful analysis of PL data is imperative to be able to pinpoint a specific defect. In particular, the BL1 band with a maximum at 2.9 eV is related to the Zn_{Ga} acceptor [21], and the BL2 band with a maximum at 3.0 eV is caused by carbon-hydrogen complexes [22].

In this paper, we present fairly plausible evidence that a new PL band with a maximum at 2.9 eV in C-doped GaN (called hereafter the BL_C band) is the sought secondary PL band of the C_N defect.

II. EXPERIMENTAL DETAILS

A. Samples

We investigated in detail PL from eight GaN samples doped with C and nine GaN samples codoped with C and Si. The samples were grown by the MOVPE method at the Institut für Physik, Magdeburg, Germany. High-purity diluted propane and silane were used for carbon and silicon doping, respectively. Other details of these samples, including growth conditions and the results of initial characterization, can be found in Ref. [23]. For nine samples, the concentration of carbon [C] exceeds the concentration of silicon [Si] according to secondary-ion mass-spectrometry (SIMS) analyses, and the samples are semi-insulating (SI). For the other eight samples, [C] < [Si] from the SIMS data, and the Hall-effect measurements show high concentrations of free electrons ($n_0 = 4 \times 10^{17}$–$6 \times 10^{18}\,\mathrm{cm}^{-3}$), which are approximately equal to the difference [Si] − [C] (Fig. 1). The samples from this second group are degenerate, n-type GaN, because the concentration of Si exceeds $10^{18}\,\mathrm{cm}^{-3}$, even though the concentration of free electrons is lower than $10^{18}\,\mathrm{cm}^{-3}$ in some of these samples.

From the fact that $n_0 \approx$ [Si] − [C] in GaN:C,Si samples and that n_0 could not be measured for samples doped with only C, we conclude that the majority of carbon atoms are deep acceptors (Si atoms act as shallow donors). Moreover, this also indicates that the concentration of donors other than Si_{Ga} (such as O_N) is negligible in the GaN:C,Si samples, and that the concentration of residual Si_{Ga} donors is relatively low

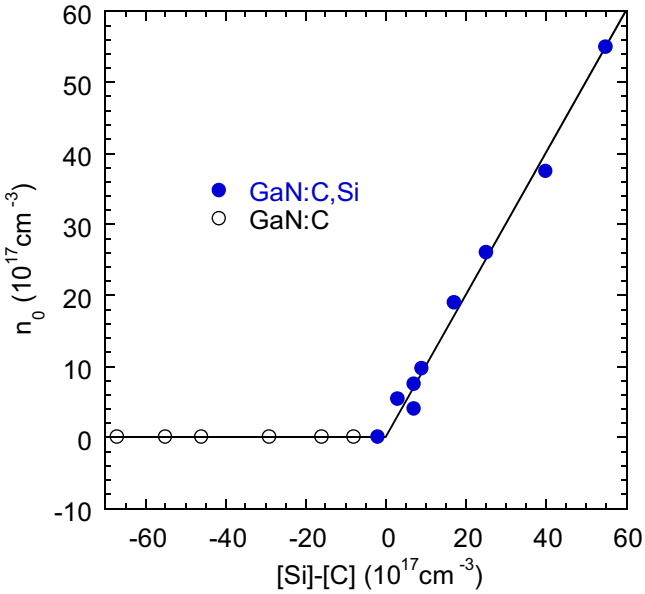

FIG. 1. The concentration of free electrons determined from Hall-effect measurements as a function of the difference between the concentrations of Si and C atoms determined from SIMS measurements for GaN:C and GaN:C,Si samples. Two semi-insulating GaN:C samples with [C] − [Si] > $10^{19}\,\mathrm{cm}^{-3}$ and $n_0 \approx 0$ are not shown in the figure.

in GaN:C samples. These conclusions are supported by the SIMS analysis of undoped reference samples, where [Si] < $10^{16}\,\mathrm{cm}^{-3}$ and [O] < $10^{17}\,\mathrm{cm}^{-3}$. The dependence shown in Fig. 1 also strongly supports the assumption that the majority of the C atoms in the studied samples are in the form of the C_N acceptors, and only a small fraction of carbon atoms may be in the form of the C_NO_N and C_NSi_{Ga} complexes, which are deep donors.

Table I summarizes the parameters of representative samples studied in more detail. These are three n-type GaN samples codoped with C and Si and having different concentrations of free electrons and one semi-insulating GaN sample doped with C (MD91). Additionally, two MOVPE GaN samples grown at other facilities are included. The undoped GaN sample (EM1256), containing small amounts of C and Si, was grown at EMCORE Corp. [24] and studied in several works [5,6,15,17]. The Si-doped GaN sample cvd3540 was grown by MOVPE at Virginia Commonwealth University.

B. Photoluminescence measurements

Steady-state PL (SSPL) was excited with an unfocused He-Cd laser (30 mW, 325 nm), dispersed by a 1200 rules/mm grating in a 0.3-m monochromator and detected by a cooled photomultiplier tube. Calibrated neutral-density filters were used to attenuate the excitation power density (P_{exc}) over the range of 10^{-7}–$0.2\,\mathrm{W/cm}^2$. For high excitation power densities, up to $200\,\mathrm{W/cm}^2$, the laser beam was focused onto a ∼0.1-mm-diameter spot. A closed-cycle optical cryostat was used for temperatures between 15 and 320 K, and a high-temperature optical cryostat was used for temperatures between 150 and 700 K.

TABLE I. Parameters of GaN samples. η_{YL1} is the absolute quantum efficiency of the YL1 band; C_{pA1} and C_{pA2} are the hole-capture coefficients for the C_N defect in the 1− and 0 charge states, respectively.

Sample number	n_0 (cm^{-3})	[Si] (cm^{-3})	[C] (cm^{-3})	η_{YL1}	C_{pA1}/C_{pA2}
MD33	9.7×10^{17}	1.5×10^{18}	6.0×10^{17}	0.85 ± 0.1	3500
MD42	7.5×10^{17}	1.4×10^{18}	7.0×10^{17}	0.8 ± 0.1	3000
MD45	3.8×10^{18}	6.0×10^{18}	2.0×10^{18}	0.6 ± 0.2	∼2000
MD91		$<10^{16}$	1.6×10^{18}	∼0.05	
EM1256	2×10^{16}	3×10^{16}	4×10^{16}	0.1–0.2	3000
cvd3540	5×10^{17}			0.5 ± 0.2	1800

All the samples were measured under identical conditions, and the PL spectra were corrected for the spectral response of the measurement system. First, a correction function has been found by comparing the measured spectrum of a calibrated tungsten lamp with the known spectral irradiance of this lamp (in units proportional to milliwatts per nanometer) as a function of light wavelength λ. Then, the measured PL spectra, $I^{PL}(\lambda)$, were multiplied by λ^3 in order to plot the spectra in units proportional to the number of emitted photons as a function of photon energy [λ^2 arises from conversion of the $I^{PL}(\lambda)$ dependence to the $I^{PL}(\hbar\omega)$ dependence [25], and additional factor λ arises from conversion of milliwatts to number of photons]. This last step was omitted in our previous publications and apparently in publications by other authors in the nitride community. As a result, the position of the YL1 band maximum reported previously (2.20 eV at 15 K and 2.22 eV at 50 K for unstrained GaN layers) [6] will redshift by 0.04–0.05 eV after multiplication of the PL spectrum by λ^3.

The absolute internal quantum efficiency of the PL, η, is defined as $\eta = I^{PL}/G$, where I^{PL} is the PL intensity (in number of photons from a particular PL band emitted from a unit volume per unit time) and G is the concentration of electron-hole pairs created by the laser per second in the same volume. To find η for a particular PL band, we analyzed temperature dependences of PL intensities in the temperature region where a PL band with very high η is quenched or, in case of low η, compared PL intensity integrated over the PL band with the integrated PL intensity obtained from calibrated GaN samples [26,27], as explained in Sec. III B.

The time-resolved PL (TRPL) was excited with a pulsed nitrogen laser (pulses with duration of 1 ns, repetition frequency of 6 Hz, and photon energy of 3.68 eV) and analyzed with a digital oscilloscope. The photon flux during the pulse, P_0, was varied between 5×10^{20} and 5×10^{23} $cm^{-2}\,s^{-1}$ by using neutral density filters. At each of the photon energies, the PL transient was measured (10 000 data points) by averaging the signal for 1–3 min. The signal measured before arrival of the pulse was considered the baseline and subtracted to allow for the PL decay to be analyzed over two to three orders of magnitude in intensity and time. The TRPL spectra were obtained from these transients at selected time delays. The stability of the signal was validated by measuring the PL decay at a characteristic photon energy (usually at the band maximum) before and after the PL spectrum measurement. Faster PL transients were measured using 266-nm excitation from a frequency tripled femtosecond Ti:sapphire laser ($2\,W/cm^2$, repetition rate tuned from 8 to 80 MHz using a pulse picker) and a Hamamatsu streak camera with 25-ps resolution in the photon counting mode.

III. RESULTS

A. Photoluminescence at low excitation intensity

The SSPL spectrum at low excitation intensity for one of the conductive n-type GaN:C,Si samples is shown in Fig. 2. The near-band-edge (NBE) emission has a maximum at 3.486 eV, and it is attributed to annihilation of excitons bound to shallow Si_{Ga} donors. The peak is shifted to higher energies by about 15 meV as compared to bulk GaN due to compressive strain in the GaN layer. A very weak ultraviolet luminescence (UVL) band is observed with the strongest peak at 3.282 eV. The main feature in the PL spectrum is the yellow luminescence (YL1) band with a maximum at ∼2.2 eV. A careful analysis of its high-energy side, similar to that reported in Ref. [6], reveals the ZPL at 2.59–2.60 eV. To analyze the

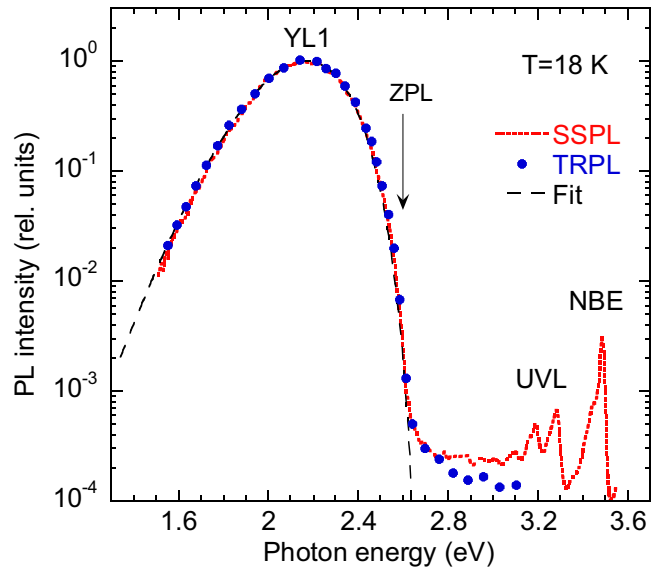

FIG. 2. Normalized PL spectrum from sample MD42 at $T = 18$ K. The thick dotted line is the SSPL spectrum taken at $P_{exc} = 0.013\,W/cm^2$ with an unfocused laser beam. The filled circles represent the TRPL spectrum taken at 10^{-5} s after a laser pulse with $P_0 = 5\times10^{22}\,cm^{-2}\,s^{-1}$ during the 1-ns pulse. The abrupt cutoff of the YL1 band at 2.6 eV agrees with the ZPL position. The dashed line is calculated using Eq. (1) with the following parameters: $E_0{}^* = 2.665$ eV, $\hbar\omega_{max} = 2.17$ eV, and $S_e = 7.7$. The NBE peak is at 3.486 eV.

shape of the YL1 band, we used the following expression obtained using a one-dimensional configuration coordinate model [28]:

$$I^{\mathrm{PL}}(\hbar\omega) = I^{\mathrm{PL}}(\hbar\omega_{\max}) \exp\left[-2S_e\left(\sqrt{\frac{{E_0}^* - \hbar\omega}{\Delta_{\mathrm{FC}}}} - 1\right)^2\right]. \quad (1)$$

Here, S_e is the Huang-Rhys factor for the excited state (when a hole is bound to the acceptor), $\Delta_{\mathrm{FC}} = {E_0}^* - \hbar\omega_{\max}$ is the Franck Condon shift, $\hbar\omega$ and $\hbar\omega_{\max}$ are the photon energy and position of the band maximum, respectively, ${E_0}^* = E_0 + 0.5\,\hbar\Omega$, E_0 is the ZPL energy, and $\hbar\Omega$ is the energy of the dominant phonon mode in the excited state.

The shape of the YL1 band remains the same in different samples, both in SSPL and TRPL measurements (Fig. 2). The YL1 band maximum and its ZPL redshift by about 30 meV with decreasing excitation power density from 0.2 to $10^{-4}\,\mathrm{W/cm^2}$. In some n-type GaN samples with high concentration of Si, the YL1 band maximum redshifted by more than 50 meV and the full width at half maximum increased by 30 meV with decreasing excitation intensity. This shift is much larger than the shift of the YL1 band in GaN samples with very low concentration of impurities (6 meV for undoped GaN) [6]. The *small* shift in high-purity samples can be explained by the donor-acceptor pair (DAP) nature of transitions that cause the YL1 band at low temperature, namely, transitions from a shallow donor to a deep acceptor [29]. The relatively *large* shift in GaN samples codoped with Si and C can be attributed to moderate potential fluctuations in a heavily doped semiconductor [30].

B. Absolute internal quantum efficiency of photoluminescence

For samples with very high internal quantum efficiency of PL, the absolute value of η for a particular PL band can be found with high accuracy with a method based on detailed analysis of PL and fitting it with a rate-equations model [26,27]. Note that this method also provides the absolute efficiency of nonradiative recombination, despite the fact that it is not directly observed in PL experiments. An example of finding η for sample MD42 is illustrated in Fig. 3, where the temperature dependences of PL are analyzed in the temperature region where the YL1 band is quenched. When the YL1 band is quenched due to escape of holes from the $\mathrm{C_N}$ acceptor to the valence band, these holes are redistributed among the other recombination channels, and intensities of all PL bands (as well as the nonradiative recombination efficiency) rise accordingly. The stepwise rise by a factor of R in the temperature dependence is uniquely related to the absolute internal quantum efficiency of the YL1 band before quenching, $\eta_{\mathrm{YL1},0}$ [26,27,31]:

$$\eta_{\mathrm{YL1},0} = \frac{R-1}{R}. \quad (2)$$

For two $I^{\mathrm{NBE}}(T)$ dependences shown in Fig. 3, $R = 5$ and 8, which results in $\eta_{\mathrm{YL1},0} = 0.80$–$0.88$. The fit of the $I^{\mathrm{NBE}}(T)$ dependences with Eq. (17) from Ref. [27] is shown with thin solid lines in Fig. 3. Quenching of the YL1 band is fitted with the following expression (shown with thick light green line) [26]:

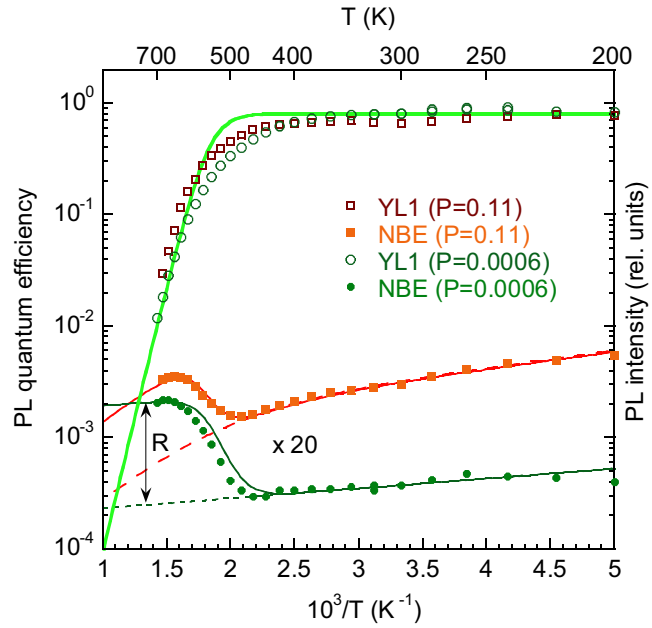

FIG. 3. Temperature dependence of the internal quantum efficiency of PL in GaN:C,Si sample MD42. $P_{\mathrm{exc}} = 0.11$ and $0.0006\,\mathrm{W/cm^2}$, as indicated in the legend. The data for the NBE band are multiplied by a factor of 20. The NBE band efficiency $\eta_{\mathrm{NBE},0}$ decreases with increasing temperature up to ~500 K. The extrapolation of this trend to higher temperatures is shown with dashed and dotted lines for two excitation intensities. The YL1 band is quenched and the NBE band rises concurrently at $T > 500$ K. From the value of the step R in this dependence, the YL1 band efficiency at temperatures before the quenching can be estimated. The thick solid green line is a fit using Eq. (3) with the following parameters: $\eta_{\mathrm{YL1},0} = 0.88$, $g = 2$, $\tau_{\mathrm{YL1}} = 100\,\mu\mathrm{s}$, $C_{pA1} = 3 \times 10^{-7}\,\mathrm{cm^3/s}$, $E_{A1} = 840\,\mathrm{meV}$.

$$\frac{I^{\mathrm{YL1}}(T)}{I^{\mathrm{YL1}}(0)} = \frac{\eta_{\mathrm{YL1}}(T)}{\eta_{\mathrm{YL1},0}} = \frac{1}{1 + (1-\eta_{\mathrm{YL1},0})\tau_{\mathrm{YL1}} C_{pA1} N_v g^{-1} \exp\left(-\frac{E_{A1}}{kT}\right)}. \quad (3)$$

Here, $I^{\mathrm{YL1}}(T)$ and $I^{\mathrm{YL1}}(0)$ are the integrated YL1 band intensities at a given temperature and in the limit of low temperatures, $\eta_{\mathrm{YL1}}(T)$ and $\eta_{\mathrm{YL1},0}$ are the corresponding internal quantum efficiencies, τ_{YL1} is the PL lifetime of the YL1 band at temperatures before its quenching, C_{pA1} is the hole-capture coefficient for the YL1-related defect, N_v is the effective density of states in the valence band, E_{A1} is the energy of the $-/0$ transition level with respect to the valence-band maximum, and k is Boltzmann's constant. Deviations of the experimental dependence from the theoretical dependence at $T \approx 400$–600 K can be explained by the spread of PL lifetimes as will be discussed in Sec. III D.

The absolute internal quantum efficiency of the YL1 band is proportional to its integrated intensity. The proportionality factor A includes the light extraction efficiency that may be different for different samples [32]. In order to determine the proportionality factor more reliably, we compared the

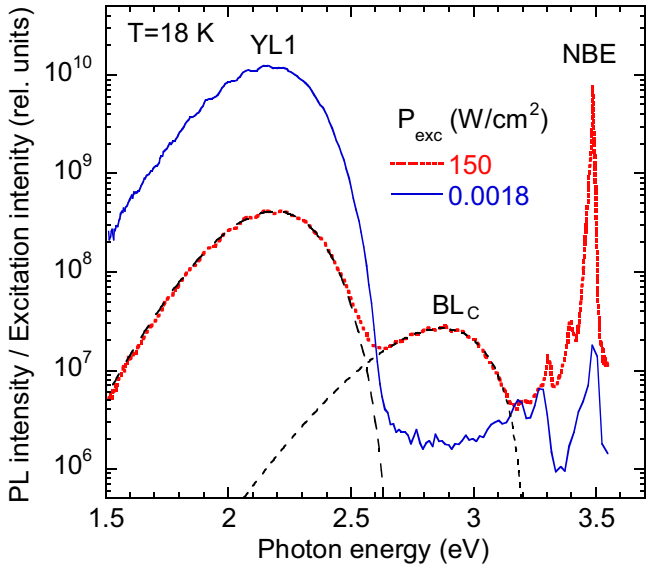

FIG. 4. The SSPL spectra for GaN codoped with C and Si (sample MD42) at low and high excitation intensity (both obtained with a focused laser beam) at $T = 18$ K. The PL intensity is divided by the excitation intensity for convenience of comparison. The dashed lines are calculated using Eq. (1) with the following parameters: $I^{\mathrm{PL}}(\hbar\omega_{\max}) = 4.1 \times 10^8$, $S_e = 7.4$, $E_0{}^* = 2.69$ eV, $\hbar\omega_{\max} = 2.19$ eV (for the YL1 band) and $I^{\mathrm{PL}}(\hbar\omega_{\max}) = 2.65 \times 10^7$, $S_e = 2.7$, $E_0{}^* = 3.2$ eV, $\hbar\omega_{\max} = 2.87$ eV (for the BL_C band).

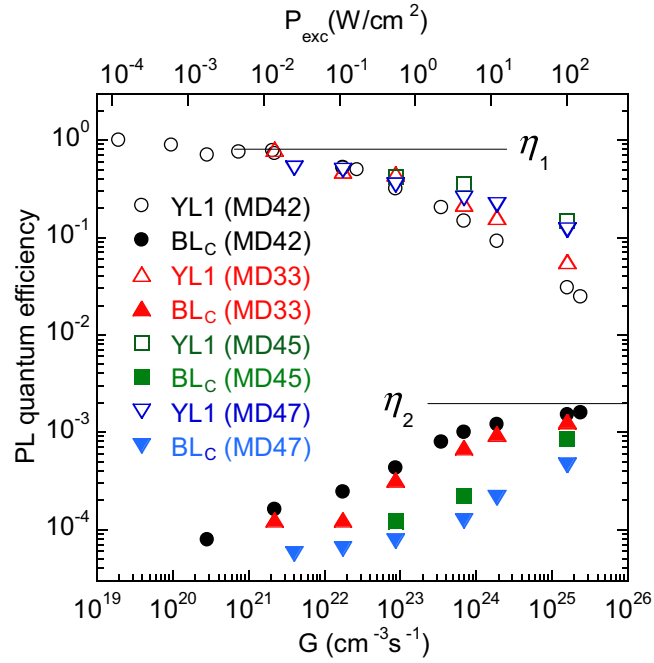

FIG. 5. PL quantum efficiency of the YL1 (η_1) and BL_C (η_2) bands in GaN:C,Si samples at 18 K as a function of excitation intensity. Note that error bars are about ±30%.

absolute internal quantum efficiency with the integrated PL intensity for four GaN:C,Si samples exhibiting $\eta > 0.6$ for which the step R in the temperature dependence (Fig. 3) could be reliably determined. The obtained factor A was similar to that obtained from other "calibration" samples (GaN:Zn,Si exhibiting strong BL1 band and GaN:Mg exhibiting strong UVL band). The standard deviation of A in a set of seven calibration samples was about 20%. The factor A was used to estimate the absolute internal quantum efficiency of PL for all other samples where no steps in the temperature dependence of PL intensity could be observed because of low quantum efficiency.

C. Steady-state photoluminescence at high excitation intensities

At excitation intensities, sufficiently high for the YL1 band intensity to saturate, a new PL band, which is labeled as the BL_C band, emerges at higher photon energies (Fig. 4). Saturation of the YL1 intensity begins at about 0.1 W/cm^2, whereas no saturation of the BL_C band (no decrease of the BL_C efficiency) is observed up to 200 W/cm^2 (Fig. 5). The BL_C band has a maximum at $\hbar\omega_{\max} \approx 2.9$ eV and can be fitted using Eq. (1) with $S_e = 2.7$ and $E_0{}^* = 3.2$ eV (Fig. 4). Although the position and shape of the BL_C band are similar to those of the BL1 band attributed to the Zn_{Ga} ($\hbar\omega_{\max} = 2.9$ eV, $S_e = 3.0$, and $E_0{}^* = 3.17$ eV) [33], we will show below that these bands originate from different defects.

Let us consider two defects, A1 and A2, which cause two PL bands with intensities I_1^{PL} and I_2^{PL} at low excitation intensities (when the defects are not saturated with photogenerated holes) in an n-type semiconductor with equilibrium concentration of free electrons n_0. By using a phenomenological model with several recombination channels, including radiative and nonradiative defects [1,26], we can express I_1^{PL} and I_2^{PL} as

$$I_1^{\mathrm{PL}} = \eta_1 G = C_{nA1} N_{A1}^0 n_0 = C_{pA1} N_{A1} p \tag{4}$$

and

$$I_2^{\mathrm{PL}} = \eta_2 G = C_{nA2} N_{A2}^0 n_0 = C_{pA2} N_{A2} p, \tag{5}$$

where η_1 and η_2 are the absolute internal quantum efficiencies of the two PL bands, G is the electron-hole pair generation rate, p is the concentration of photogenerated holes, N_{Ai}^0 and N_{Ai} are the concentration of bound holes at defects i and the total concentration of these defects, respectively, and C_{nAi} and C_{pAi} are the capture coefficients for electrons and holes, respectively, by defect i. In Eqs. (4) and (5), we assume that the defects are not saturated with photogenerated holes ($N_{Ai}^0 \ll N_{Ai}$). After dividing Eq. (4) by Eq. (5), we obtain

$$\frac{\eta_2}{\eta_1} = \frac{C_{pA2} N_{A2}}{C_{pA1} N_{A1}}. \tag{6}$$

With increasing G, I_i^{PL} increases linearly until the defects of type i become saturated with photogenerated holes, after which I_i^{PL} does not increase according to the *simple* model. In this model [26], electron-hole pairs are generated uniformly in a volume with effective thickness $d = \alpha^{-1}$ near the sample surface, where α is the absorption coefficient of GaN at the photon energy of the HeCd laser ($\alpha \approx 10^5$ cm^{-1}). The critical generation rates, G_{01} and G_{02}, at which the linear rises for the

TABLE II. The capture coefficients for defects responsible for major defect-related PL bands in GaN.

PL band	C_{nA} (cm^3/s)	C_{pA} (cm^3/s)
UVL	$(3.2 \pm 0.3) \times 10^{-12}$	$(1.0 \pm 0.3) \times 10^{-6}$
BL1	$(6.8 \pm 0.7) \times 10^{-13}$	$(4.9 \pm 1.4) \times 10^{-7}$
BL_C	$\sim 1 \times 10^{-9}$	$\sim 1 \times 10^{-10}$
YL1	$(1.1 \pm 0.1) \times 10^{-13}$	$(3.7 \pm 1.6) \times 10^{-7}$
RL1	$(4.3 \pm 0.4) \times 10^{-14}$	$(2.9 \pm 0.7) \times 10^{-7}$

two PL bands change into a complete saturation, can be found from Eqs. (4) and (5) as

$$G_{01} = \frac{C_{nA1} N_{A1} n_0}{\eta_1} \tag{7}$$

and

$$G_{02} = \frac{C_{nA2} N_{A2} n_0}{\eta_2}. \tag{8}$$

The ratio G_{01}/G_{02} can be found from Eqs. (6)–(8) as

$$\frac{G_{01}}{G_{02}} = \frac{C_{nA1} C_{pA2}}{C_{nA2} C_{pA1}}. \tag{9}$$

The parameters C_{nAi} and C_{pAi} are deduced from experimental data for the main PL bands in GaN and listed in Table II [1,32,33]. In addition to the PL bands discussed in this paper, the RL1 band with a maximum at 1.8 eV is included, because for all these bands PL is caused by electron transitions from the conduction band (at elevated temperatures) to defect levels. Other PL bands, such as RL2, RL3, GL1, GL2, and BL2, are caused by internal transitions (i.e., from an excited state to the ground state of the same defect) [18,28,33,51]. In case of such internal transition, the electron has already been captured by the defect prior to the optical transition, and the value of C_{nAi} cannot be extracted from the PL lifetime.

By using Eq. (9) and the data from Table II, we find that the G_{01}/G_{02} ratios for the UVL, BL1, YL1, and RL1 bands are not more than an order of magnitude different from unity. For example, $G_0(\text{UVL})/G_0(\text{BL1}) = 2.3$ and $G_0(\text{BL1})/G_0(\text{YL1}) = 4.7$. This means that saturation of these PL bands should begin at about the same excitation intensity (within an order of magnitude), which is confirmed experimentally [32,34]. In striking contrast, the $G_0(\text{BL}_C)/G_0(\text{YL1})$ ratio is at least 10^3–10^4, as can be seen from Fig. 5. This indicates that the defect responsible for the BL_C band has a small hole-capture cross section and a large electron-capture cross section as compared to acceptors responsible for the dominant PL bands in GaN, including the BL1 band. Thus, the BL_C and BL1 are clearly not the same PL band in nature, as could be erroneously concluded from observing similar PL band positions and shapes. Moreover, we conclude that the BL_C band is an excellent candidate for the long-sought secondary PL band of the C_N defect, as will be justified below.

Indeed, at low excitation intensities, most of the C_N acceptors are filled with electrons (C_N^-) in *n*-type GaN:C,Si. After a C_N^- acceptor captures a photogenerated hole from the valence band, it becomes neutral (C_N^0). The capture of the hole is very fast (large C_{pA1}), because of Coulomb attraction between the negatively charged acceptor and a positively charged hole. The fast capture of holes is responsible for high quantum efficiency of the associated YL1 band, η_1 [see Eq. (4)]. The YL1 band is caused by transitions of electrons from the conduction band to the $-/0$ level of the C_N defects at elevated temperatures ($T > 50$ K). This transition is "slow" (small C_{nA1}), because the electrons are captured by a neutral defect, and the PL lifetime is inversely proportional to C_{nA1} and n_0. With increasing excitation intensity in SSPL, the concentration of the C_N defects with bound holes increases and eventually all the C_N defects become saturated with photogenerated holes ($C_N^0 \approx C_N$) at $G = G_{01}$. The capture of a second hole by the C_N defect in a neutral charge state, resulting in conversion of C_N^0 into C_N^+, should be slow (small C_{pA2}). Finally, the radiative recombination of a free electron with one of the holes at the C_N^+ is expected to be very fast (large C_{nA2}) due to its attractive character. Thus, we propose that the electron transition from the conduction band to the $0/+$ level of the C_N defect causes the BL_C band. The quantum efficiency of the BL_C band is very low ($\eta_2 \ll \eta_1$), because $C_{pA2} \ll C_{pA1}$, and the BL_C lifetime is very short, because $C_{nA2} \gg C_{nA1}$. The C_{pA2} for the new PL band can be found from rate equations similar to Eqs. (4) and (5) with $N_{A1} = N_{A2}$ as

$$C_{pA2} \approx R \frac{\eta_2}{\eta_1} C_{pA1}, \tag{10}$$

where η_1 should be taken for $G < G_{01}$, and η_2 should be taken for $G_{01} < G < G_{02}$. The factor R appears because the quantum efficiency of the YL1 band decreases due to saturation of the C_N defects with holes, while efficiencies of all other PL bands (as well as nonradiative recombination efficiency) increase by a factor of R for $G_{01} < G < G_{02}$, very similar to the increase of the NBE intensity in Zn-doped GaN samples [27]. According to the data shown in Fig. 5, $\eta_1/\eta_2 \approx 400$. With $C_{pA1} = 3.7 \times 10^{-7}$ cm^3/s for the YL1 band, and $R \approx 5$–8 for this sample, we estimate $C_{pA2} \approx 1 \times 10^{-10}$ cm^3/s for the BL_C band.

We observed the BL_C band emerging at high excitation intensities in all eight conductive, *n*-type GaN:C,Si samples discussed in this paper. In some samples, the C_{pA1}/C_{pA2} ratio was close to 500; in others it was larger (1000–2000), because the BL_C efficiency has not reached saturation (i.e., $G < G_{01}$) (Fig. 5). At $G < G_{01}$, the BL_C intensity is expected to increase superlinearly with excitation intensity, because in this excitation region the probability that two holes will be captured by a particular defect in time shorter than the PL lifetime is proportional to the square of the excitation intensity [35]. We can see that the quantum efficiency of the BL_C band is very low at $G < G_{01}$, where the quantum efficiency of the YL1 band is high and constant. At $G > G_{01}$, the YL1 band efficiency decreases with excitation intensity, while the BL_C band efficiency reaches its maximum.

We now address the question why the BL_C band has not been discovered earlier. The reason is that this emission is very weak in typical conditions used for PL measurements. Moreover, in less pure samples or samples with low concentrations of C, it can be obscured by stronger PL bands

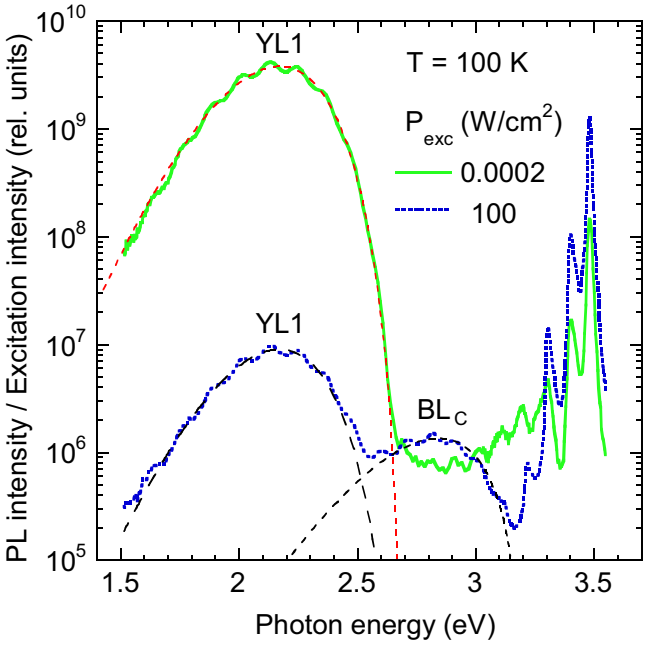

FIG. 6. The SSPL spectra for undoped GaN (sample EM1256) at low and high excitation intensity at $T = 100$ K. The PL intensity is divided by the excitation intensity for convenience of comparison. The lines are calculated using Eq. (1) with the following parameters: $I^{\mathrm{PL}}(\hbar\omega_{\max}) = 3.8 \times 10^9$ and 9×10^6, $S_e = 7.4$, $E_0{}^* = 2.68$ eV, $\hbar\omega_{\max} = 2.17$ eV (for the YL1 band) and $I^{\mathrm{PL}}(\hbar\omega_{\max}) = 1.35 \times 10^6$, $S_e = 2.7$, $E_0{}^* = 3.18$ eV, $\hbar\omega_{\max} = 2.84$ eV (for the BL_C band).

such as the UVL, BL1, or exciton emission. In n-type GaN samples discussed in this paper, the UVL band is very weak (Fig. 2) due to low contamination with Mg. By using the approach described in Ref. [32], we estimate that the concentration of Mg (responsible for the UVL band) is about 2×10^{14} cm^{-3} in sample MD42, and the concentration of Zn (responsible for the BL1 band) is lower than 2×10^{14} cm^{-3}. In semi-insulating GaN, the carbon-hydrogen complex-related BL2 band [22] covers the BL_C band, as described in Sec. III F.

Nevertheless, we were able to find the BL_C band in samples where it was not noticed initially. Previously, we investigated an undoped GaN sample contaminated with C (sample EM1256 with [C] $= 3 \times 10^{16}$ cm^{-3}, $n_0 = 2 \times 10^{16}$ cm^{-3} at room temperature, and $\eta_1 \approx 0.2$) [15,17]. From the fact that no secondary PL band emerged after the YL1 band quenched (Fig. 2 in Ref. [17]) we concluded that the YL1 band was caused by the C_NO_N complex, for which the secondary band was not expected. However, as part of the current study, we performed the measurements on the same sample again but at notably higher excitation intensities obtained with a focused laser beam and at elevated temperatures to reduce the contribution of the NBE band. Doing so revealed the BL_C band at high excitation intensities (Fig. 6). This band cannot be the BL1 band because its saturation does not begin even at the highest excitation intensity.

From relative efficiencies of the YL1 band (at $P_{\mathrm{exc}} = 0.0002$ W/cm^2) and the BL_C band (at $P_{\mathrm{exc}} = 100$ W/cm^2) we estimate $\eta_2/\eta_1 \approx 0.0003$, which agrees with the above-mentioned $C_{pA2} \approx 1 \times 10^{-10}$ cm^3/s. Similar results were obtained for Si-doped GaN sample cvd3540 (Table I), for which the BL_C band was also overlooked in the earlier preliminary study [6]. From the fact that no saturation of the BL_C band is observed at high excitation intensities, we expect that the PL lifetime for the BL_C band is much shorter than that for the dominant defect-related PL bands in GaN. To verify this prediction, we conducted TRPL measurements by using two different setups (Sec. II B), as discussed below.

D. Time-resolved photoluminescence excited with a nitrogen laser

The room-temperature YL1 intensity transients after laser pulses at several excitation intensities ($P_0 = 5 \times 10^{20}$–5×10^{23} cm^{-2} s^{-1}) are shown in Fig. 7(a). At lower temperatures (not shown), down to 18 K, the PL decays are very similar to the room-temperature data. The decays in Fig. 7(a) are not exponential, indicating the presence of diagonal transitions that may be caused by potential fluctuations or electric field in the near-surface depletion region. In this case, the effective PL lifetime, τ^* can be defined as a characteristic time for which the product of PL intensity $I^{\mathrm{PL}}(t)$ and time t has a maximum [36,37]. As can be seen from Fig. 7(b), with increasing P_0 from 5×10^{20} to 5×10^{23} cm^{-2} s^{-1}, τ^* decreases from ~200 to 25 μs.

Such behavior of the PL data can be attributed to potential fluctuations in a heavily doped semiconductor rather than just to DAP transitions. In undoped GaN, the decay of the YL1 band is nearly exponential at room temperature, and the PL lifetime is inversely proportional to the concentration of free electrons [33]. For the concentration of free electrons $n_0 = 7.5 \times 10^{17}$ cm^{-3}, obtained for sample MD42 from Hall-effect measurements, the PL lifetime for transitions from the conduction band to the YL1 defect should be

$$\tau_1 = \frac{1}{n_0 C_{nA1}} \approx 12\,\mu\mathrm{s}, \tag{11}$$

where $C_{nA1} = 1.1 \times 10^{-13}$ cm^3/s is the electron-capture coefficient for the YL1 defect [33]. With increasing excitation intensity, potential fluctuations are screened, and τ^* approaches τ_1.

The TRPL spectra taken at different time delays at room temperature are shown in Fig. 8, where they are compared with SSPL spectra. For very short time delays, about 1–10 ns, the BL_C band can be observed, for which the decay is very fast. The decay of the YL1 band begins only after 1-μs delay.

The TRPL spectra at $T = 18$ K are shown in Fig. 9. The shapes of the BL_C band in TRPL and SSPL spectra are similar. Low time resolution (~10 ns) of our TRPL setup with a nitrogen pulse laser does not allow a detailed analysis of fast decays of the BL_C band. In order to resolve this problem, additional time-resolved measurements were conducted using a femtosecond Ti-sapphire laser and a streak camera, the data for which are discussed in the following section.

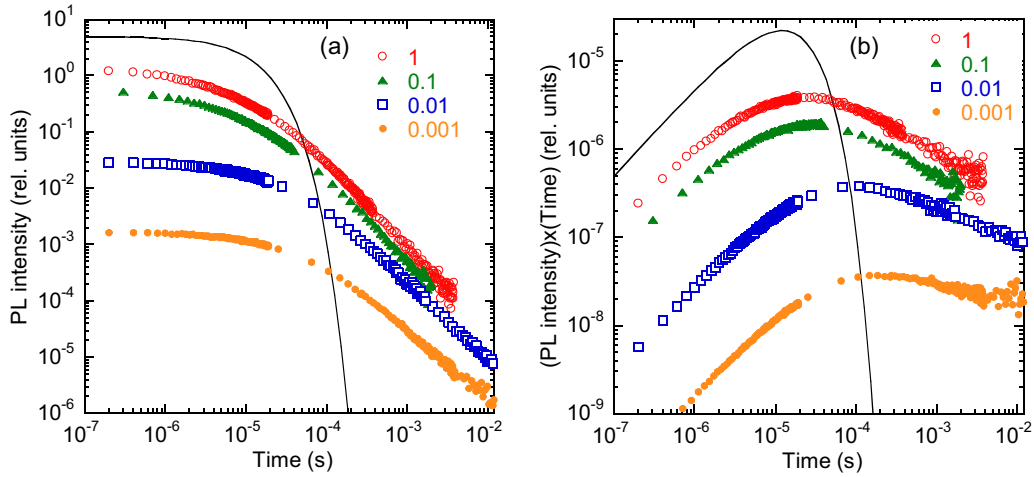

FIG. 7. The PL transients at 2.2 eV and $T = 295$ K for sample MD42. (a) PL intensity. (b) Product of PL intensity and time. The highest excitation intensity is $P_0 = 5 \times 10^{23}$ cm^{-2} s^{-1}. Attenuation of this intensity is indicated with numbers in the legend. The symbols show every 100th point. The solid curve is the exponential decay with the characteristic time $\tau_1 = 12\,\mu$s.

E. Time-resolved photoluminescence excited with a Ti-sapphire laser

The decays of the BL_C band after excitation with the femtosecond Ti-sapphire laser at $T = 15$ K are shown in Fig. 10. The decays can be fitted with the following monoexponential law:

$$I_2^{PL}(t) = I_2^{PL}(0)\exp(-t/\tau_2), \tag{12}$$

where τ_2 is the BL_C lifetime. The exponential decay of PL in an n-type semiconductor can be observed in two cases: (i) for transitions from the conduction band to a defect level [37] and (ii) for internal transitions, i.e., for transitions from an excited state to the ground state of the same defect [18]. In the first case (e-A-type transitions), the PL lifetime is inversely proportional to the concentration of free electrons:

$$\tau_2 = \tau_{eA2} = \frac{1}{n_0 C_{nA2}}, \tag{13}$$

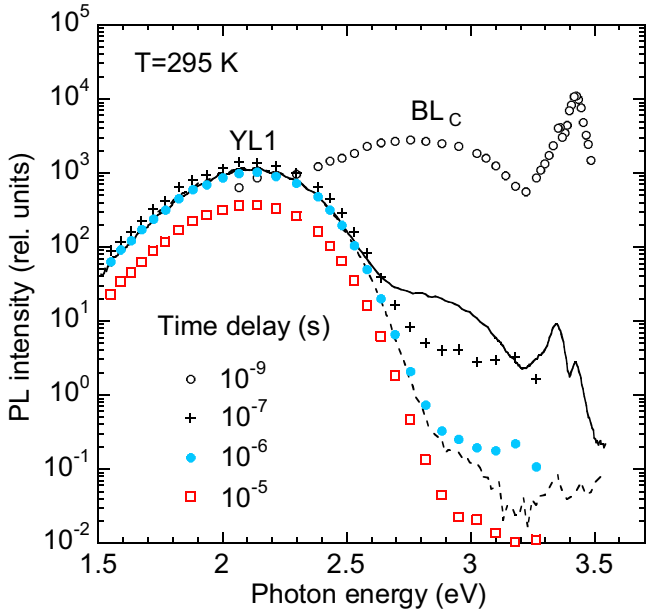

FIG. 8. PL spectra from GaN:C,Si (sample MD42) at $T = 295$ K. The symbols show the TRPL spectra at different time delays between 10^{-9} and 10^{-5} s. The SSPL spectra at $P_{exc} = 150$ and 0.025 W/cm^2, shown with the solid and dashed lines, respectively, are arbitrarily shifted vertically to match the TRPL spectrum of the YL1 band.

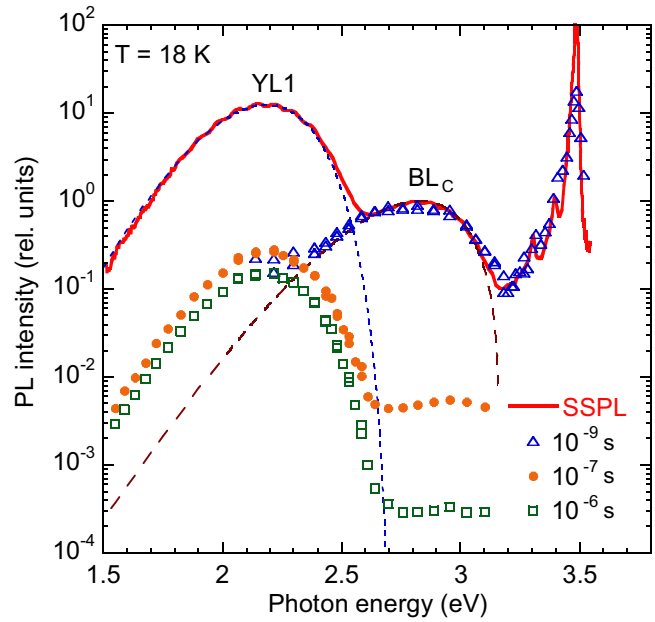

FIG. 9. Comparison of SSPL ($P_{exc} = 150$ W/cm^2) and TRPL (at indicated time delays) spectra for GaN:C,Si (sample MD42) at $T = 18$ K. The SSPL and TRPL (1 ns) spectra are normalized at the maximum of the BL_C band. The dashed lines are calculated using Eq. (1) with the following parameters: $I^{PL}(\hbar\omega_{max}) = 12.4$, $S_e = 7.4$, $E_0{}^* = 2.69$ eV, $\hbar\omega_{max} = 2.185$ eV (for the YL1 band) and $I^{PL}(\hbar\omega_{max}) = 1$, $S_e = 2.7$, $E_0{}^* = 3.16$ eV, $\hbar\omega_{max} = 2.83$ eV (for the BL_C band).

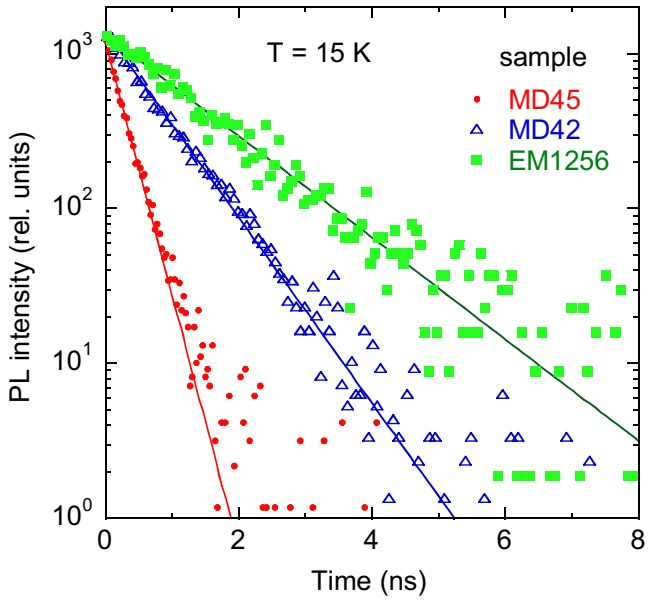

FIG. 10. PL transients for n-type GaN samples at $T = 15$ K and $\hbar\omega = 2.9$ eV. Every 3rd point is shown. The lines are fits using Eq. (12) with the following parameters: $\tau_2 = 0.27$ ns (sample MD45), $\tau_2 = 0.72$ ns (sample MD42), $\tau_2 = 1.32$ ns (sample EM1256).

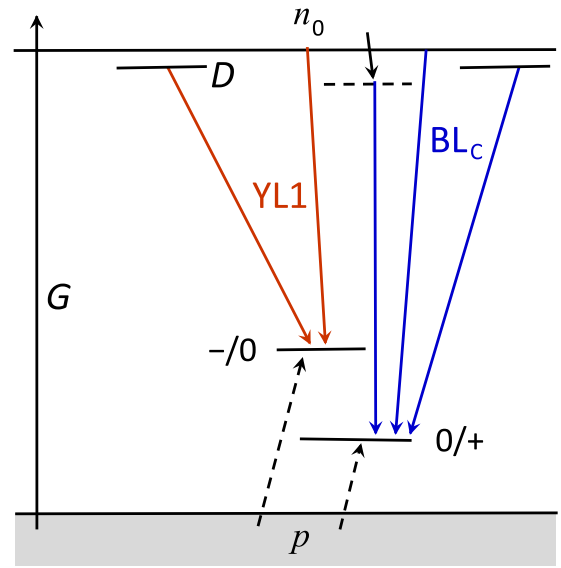

FIG. 11. Schematic band diagram showing the main transitions in GaN:C,Si. The upward arrow, G, shows the band-to-band excitation. The solid and dashed arrows show the transitions of electrons and holes, respectively. The YL1 band is caused by transitions of electrons from shallow donor levels, D, or from the conduction band to the $-/0$ level of the C_N defect. The BL_C band is caused by electron transitions from the conduction band, shallow donors, or from an excited state (depicted as the dashed horizontal bar) to the $0/+$ level of the C_N.

whereas in the second case the PL lifetime is independent of n_0. For the BL_C band, the PL lifetime of the BL_C band for sample MD45 ($\tau_2 = 0.27$ ns) is about three times shorter than that for sample MD42 ($\tau_2 = 0.72$ ns). This roughly agrees with Hall effect measurements, according to which the room-temperature concentration of free electrons in sample MD45 ($n_0 = 3.8 \times 10^{18}\,\mathrm{cm}^{-3}$) is five times higher than in sample MD42 ($n_0 = 7.5 \times 10^{17}\,\mathrm{cm}^{-3}$). However, for sample EM1256 with a free-electron concentration two orders of magnitude lower than that for the GaN:C,Si samples (Table I), an exponential decay of the BL_C band is observed with the lifetime of $\tau_2 = 1.32$ ns, which is much shorter than expected from Eq. (13). The decay time for this sample increased only slightly with temperature, from 1.32 ns at 15 K to 1.67 ns at 100–150 K.

To explain this apparent disagreement, we suggest that transitions via an excited state and directly from the conduction band compete with each other (Fig. 11). The excited hydrogenlike state originates from Coulomb potential of the positively charged C_N. The characteristic time, τ_e, for the capture of free electrons by this state is very short, since it is expected to behave as a giant trap. The internal transition from this state to the ground state $0/+$ has a characteristic time τ_0, which is independent of n_0 and nearly independent of temperature. A competing recombination channel is that of an electron transition from the conduction band directly to the ground state $0/+$ with the characteristic time τ_{eA2}. For the former channel, the PL will decay after a pulse with a characteristic time approximately equal to the longer of τ_e and τ_0 when the difference between the two is large [18]. On the other hand, both of these channels act in parallel, and the fastest channel would dominate (the DAP-type transition can be ignored, being much slower). Thus, the overall PL lifetime, τ_2, measured in TRPL experiments can be found from the following expression:

$$\frac{1}{\tau_2} \approx \frac{1}{\tau_{eA2}} + \frac{1}{\tau_e + \tau_0}. \tag{14}$$

In samples with low concentration of free electrons (such as EM1256), $\tau_{eA2} \gg \tau_0 > \tau_e$, and $\tau_2 \approx \tau_0$. In samples with high concentration of free electrons, $\tau_0 \gg \tau_e, \tau_{eA2}$, and $\tau_2 \approx \tau_{eA2}$.

An alternative explanation of the very fast PL and a moderate dependence of the PL lifetime on n_0 for the BL_C band can also be offered. It is possible that e-A transitions for the BL_C band are much slower than 1 ns, and we observe only internal transitions with $\tau_2 \approx \tau_0$. The decrease of τ_0 in samples with high concentrations of C and Si can be explained in this case by the energy transfer, i.e., photon reabsorption when PL emission band overlaps with the absorption band of another defect [38]. Indeed, not only n_0 is the highest in sample MD45 among analyzed samples, but also the concentrations of C and Si (Table I). A similar effect was previously observed for internal transitions in the N3 center in diamond [39]. The PL from internal transitions in the N3 center decreased from 41 to 18 ns with increasing concentration of pairs of nitrogen atoms in different samples.

We analyzed TRPL at different temperatures, excitation intensities, and photon energies. The PL lifetimes were independent of excitation power density (between 0.2 and 2 $\mathrm{W/cm}^2$) and photon energy (between 2.7 and 3.0 eV) and showed almost no variation with temperature ($\tau_2 = 0.72$, 0.25, and 1.32 ns at $T = 15$ K and $\tau_2 = 0.76$, 0.27, and 1.67 ns at

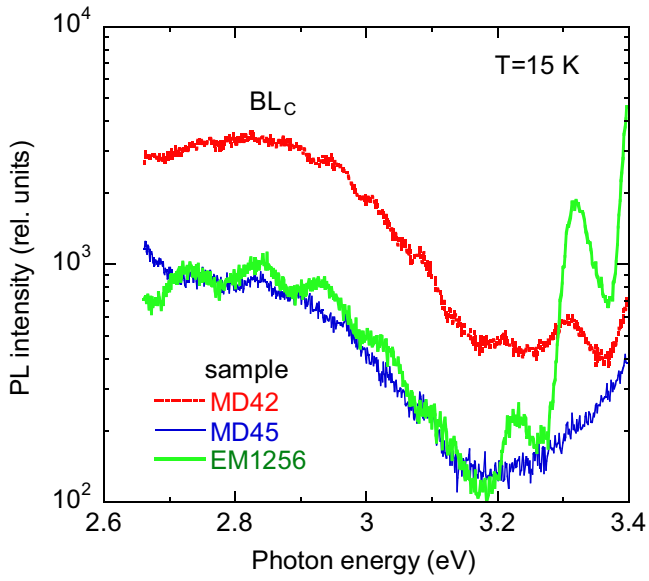

FIG. 12. Time-integrated (within 10 ns starting with the excitation pulse) PL spectra for n-type GaN:C,Si samples at $T = 15$ K.

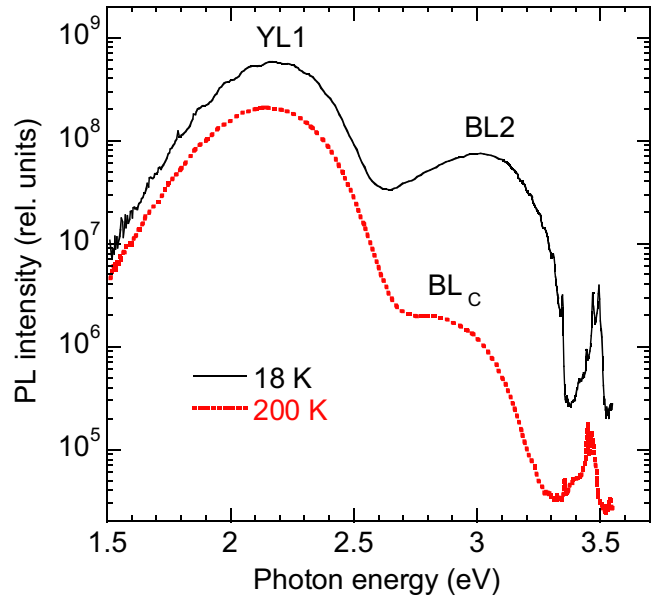

FIG. 13. SSPL spectra for semi-insulating GaN:C (sample MD91) at $P_{exc} = 0.2\,\mathrm{W/cm^2}$ and different temperatures.

$T = 150$ K for samples MD42, MD45, and EM1256, respectively). The lack of discernable temperature dependence of τ_2 in samples MD42 and MD45 is explained by the fact that both samples are degenerate, and the concentration of electrons does not change with temperature. For sample EM1256, the weak temperature dependence of τ_2 may follow the temperature dependence of τ_0.

In analyses of PL decays, it is important to ensure that the decay in question corresponds to a particular PL band. The time-integrated PL spectra at $T = 15$ K for selected samples are shown in Fig. 12. These spectra support the assertion that the emission with $\tau_2 \approx 0.72$ ns (sample MD42), 0.25 ns (MD45), and 1.32 ns (EM1256) belongs to the BL$_C$ band with a maximum at about 2.9 eV. Finally, we can estimate from Eqs. (13) and (14) that $C_{nA2} \approx 1 \times 10^{-9}\,\mathrm{cm^3/s}$.

F. Photoluminescence in semi-insulating GaN:C

All the GaN samples in this paper for which [C] > [Si] are semi-insulating (Fig. 1). Because the difference between [C] and [Si] in the majority of these samples greatly exceeds the typical concentrations of unintentionally introduced point defects, it is safe to assume that the concentration of shallow donors (Si_{Ga}) and other unintentional donors (including O_N) is much smaller than the concentration of C_N acceptors. In this case, the Fermi level is close to the $-/0$ level of C_N, and a significant portion of the C_N acceptors is in the neutral charge state in dark.

In SSPL spectra of all these samples, two defect-related bands were observed, namely, the YL1 and BL2 bands. The BL2 band, with a maximum at 3.0 eV and the ZPL at 3.33 eV, was previously attributed to a carbon-hydrogen complex, either $C_NO_NH_i$ or C_NH_i [22]. We will show below that the C_NH_i is more likely. The characteristic feature of the BL2 band is its bleaching under UV exposure. Namely, the BL2 band intensity decreases with time, while the YL1 intensity rises simultaneously. Such behavior is explained by photoinduced defect reaction in which the C_NH_i responsible for the BL2 band dissociates, and remaining C_N causes the YL1 band [22].

The C_NH_i defect is a very deep donor, with the $0/+$ level at about 0.15 eV above the valence-band maximum [22]. When the Fermi level is near the $-/0$ level of the C_N (0.916 eV above the valence band), all the C_NH_i donors are in the neutral charge state. Then, only the donors with energy levels above the $-/0$ level of the C_N (Si_{Ga} and O_N), with a total concentration N_D, will compensate the C_N acceptors so that $N_A{}^- \approx N_D$ and $N_A{}^0 \approx N_A - N_D$, where N_A is the concentration of the isolated C_N defects: $N_A = [C_N] = [C] - [C_NH_i]$. Equations (4) and (5) for this case will transform into

$$I_1^{PL} = \eta_1 G = C_{nA1}(N_A - N_D)n = C_{pA1}N_D p \qquad (15)$$

and

$$I_2^{PL} = \eta_2 G = C_{nA2}N_A^+ n = C_{pA2}(N_A - N_D)p, \qquad (16)$$

where $N_A{}^+$ is the concentration of $C_N{}^+$ ($C_N{}^+ \ll C_N$, because it is difficult to saturate the $C_N{}^+$ defects with holes). After dividing Eq. (15) by Eq. (16), we obtain

$$\frac{\eta_1}{\eta_2} = \frac{C_{pA1}N_D}{C_{pA2}(N_A - N_D)}. \qquad (17)$$

Thus, the relative contribution of the BL$_C$ band in the PL spectrum (η_2/η_1) is expected to be higher in these semi-insulating samples than in conductive n-type GaN:C,Si samples if $N_A \gg N_D$. More importantly, the BL$_C$ band with relatively high quantum efficiency, η_2, can be observed at an arbitrarily low excitation intensity in this case, because the relation (17) holds in the limit of low excitation intensities.

Figure 13 shows SSPL spectra from a representative semi-insulating GaN:C sample at 18 and 200 K. At $T = 18$ K, the

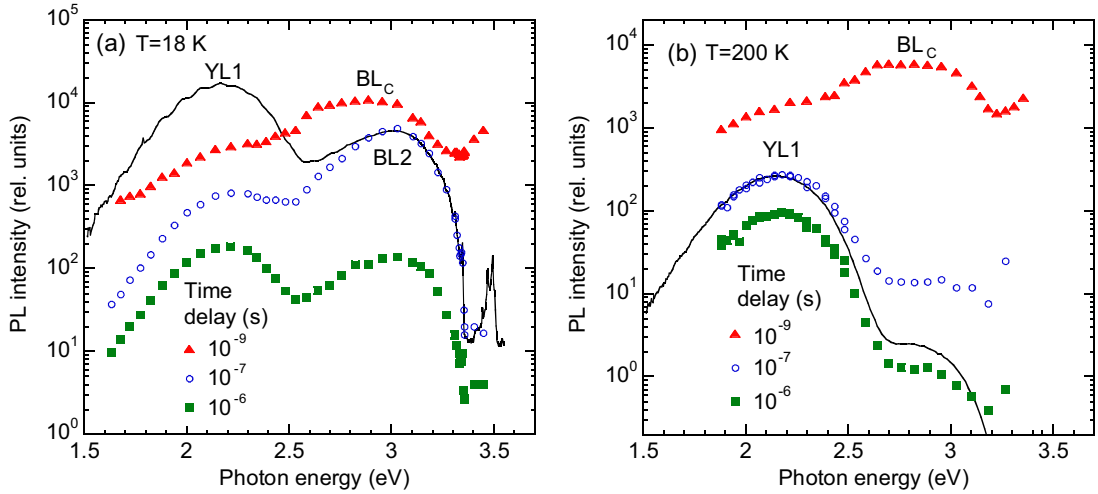

FIG. 14. TRPL spectra for semi-insulating GaN:C (sample MD91) at $P_0 = 5 \times 10^{22}\,\mathrm{cm^{-2}\,s^{-1}}$. (a) $T = 18\,\mathrm{K}$. (b) $T = 200\,\mathrm{K}$. Symbols are TRPL spectra taken in identical conditions at different times after the nitrogen laser pulse. Solid lines are SSPL spectra arbitrary shifted vertically to match a particular TRPL spectrum.

BL2 band with a maximum at 3.0 eV and the ZPL at 3.33 eV is strong. No shift of the ZPL (within ±0.2 meV) was observed when the excitation intensity was varied by a factor of 1000. The decay of the BL2 band after a laser pulse is nearly exponential, with a characteristic lifetime of about 0.3 μs. These features indicate that the BL2 band is most likely caused by an internal transition from an excited hydrogenlike state close to the conduction band to a deep donor level located at 0.15 eV above the valence band. As in other semi-insulating GaN:C samples, the bleaching of the BL2 band under prolonged UV illumination was accompanied by the rise of the YL1 band in this sample. The BL2 band is quenched at temperatures above 70 K with the activation energy of 0.15–0.20 eV (not shown) and completely disappears by 150–200 K.

Another blue band with a maximum at 2.9 eV can be seen at $T = 200\,\mathrm{K}$ (Fig. 13). Previously, we attributed this band to the Zn_{Ga} acceptor (the BL1 band) [40]. We will show below that in fact it is the BL_C band with the properties determined above. With increasing P_{exc} from $\sim 10^{-5}$ to $100\,\mathrm{W/cm^2}$, the relative efficiency (I^{PL}/P_{exc}) of the BL_C band gradually increases, by one order of magnitude in the whole range. In the same excitation intensity range, the YL1 band efficiency decreases by a factor of 30. Such behavior agrees well with the model proposed here.

The YL1 band intensity is higher than that of the BL_C band by about two orders of magnitude at low excitation intensities. By using Eq. (17) with the capture coefficients found from the analyses of conductive GaN:C,Si samples, we estimate that $N_A/N_D \approx 10$ in the GaN:C sample MD91. This estimate agrees with our expectations that $[Si_{Ga}] + [O_N]$ is equal to or less than $10^{17}\,\mathrm{cm^{-3}}$ and $[C_N]$ is equal to or less than $10^{18}\,\mathrm{cm^{-3}}$ in this sample. TRPL data discussed below support the assertion of PL features in these samples to the BL_C and BL2 bands.

The TRPL spectra obtained from the semi-insulating GaN:C sample are shown in Fig. 14. At $T = 18\,\mathrm{K}$, the BL2 and YL1 bands are observed at relatively long time delays after a laser pulse (10^{-7}–10^{-6} s). At very short time delays (a few nanoseconds), it is difficult to resolve the BL2 and BL_C bands [Fig. 14(a)]. However, the BL_C band decays very quickly, leaving the BL2 band alone by 10^{-7} s. The TRPL spectrum at this long time delay is identical to the SSPL spectrum, including the ZPL at 3.33 eV [Fig. 14(a)]. The decay of the BL2 band is nearly exponential, with the characteristic lifetime of about 200–400 ns. With increasing temperature, the BL2 band is quenched and disappears, so that only the BL_C and YL1 bands can be observed at $T = 200\,\mathrm{K}$ [Fig. 14(b)]. Another TRPL setup was used to analyze faster transients, as discussed below.

Figure 15 shows the PL spectra obtained using 266-nm excitation from the frequency tripled Ti-sapphire laser. The PL decay at $T = 15\,\mathrm{K}$ is biexponential, which can be fitted with the following expression:

$$I^{PL}(t) = I_2^{PL}(0)\exp(-t/\tau_2) + I_3^{PL}(0)\exp(-t/\tau_3), \quad (18)$$

with $\tau_2 = 2.47\,\mathrm{ns}$ and $\tau_3 = 45\,\mathrm{ns}$. The fast and slow components correspond to the BL_C and BL2 bands, respectively [41]. This attribution is confirmed by analysis of time-integrated spectra at different time delays: the band maximum shifts from ~2.9 eV immediately after the excitation pulse ($t = 0$) to ~3.0 eV at $t = 10\,\mathrm{ns}$. The slow component could be observed even after several hundred nanoseconds, in agreement with results obtained with a nitrogen laser.

IV. DISCUSSION

In this section, we will discuss the properties of the C_N defect and compare the experimental results with the results of first-principles calculations. Identity of defects responsible for the YL1, GL1, BL_C, and BL2 bands in undoped and C- and Si-doped GaN grown by HVPE will also be discussed.

A. Concentration of defects responsible for the YL1 band

Our conclusions about the origin of the YL1 band were mostly based so far on theoretical predictions and on comparison of the electrical properties of samples with the SIMS data

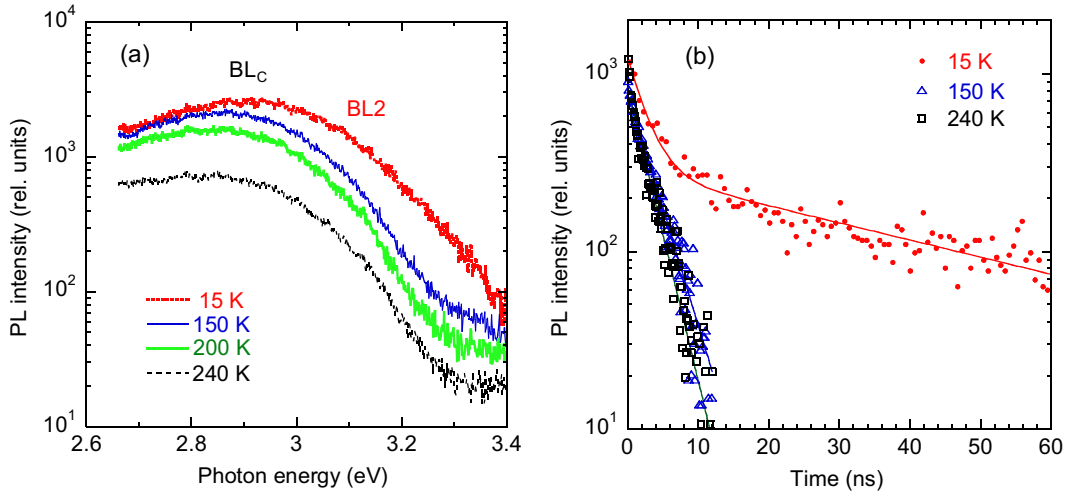

FIG. 15. TRPL at different temperatures obtained using a Ti-sapphire laser (excitation at 266 nm) for the semi-insulating GaN:C sample (MD91). (a) Time-integrated PL spectra. (b) PL transients near 2.95 eV. The decay at 15 K is fitted using Eq. (18) with $\tau_2 = 2.47$ ns and $\tau_3 = 45$ ns.

(Fig. 1). However, the concentration of defects responsible for the YL1 band can also be estimated from PL analysis and compared with the SIMS data. Estimates of the concentrations can be obtained independently from the SSPL and TRPL dependences on excitation intensity [32,37], as will be shown below.

The PL intensity from defects increases linearly with the electron-hole generation rate G until the defects become saturated with photogenerated holes. Both in SSPL and TRPL, the linear dependence $I^{\mathrm{PL}}(G)$ changes into a sublinear dependence (often close to $G^{1/2}$) above the characteristic generation rate G_{01} (Fig. 16). In case of SSPL,

$$G_{01} = \frac{N_1}{\eta_{10}\tau_1}, \tag{19}$$

whereas, in case of TRPL,

$$G_{01} = \frac{N_1}{\eta_{10} t_L}, \tag{20}$$

where η_{10} is the absolute internal quantum efficiency of the YL1 band in the limit of low excitation intensities, τ_1 is the YL1 lifetime, N_1 is the concentration of defects responsible for the YL1 band, and t_L is the length of the laser pulse [37].

From the SSPL data [Fig. 16(a)], by taking $\eta_{10} = 0.15$, $\tau_1 = 0.4$ ms, and $G_{01} = 2 \times 10^{20}\,\mathrm{cm^{-3}\,s^{-1}}$ for sample EM1256, we obtain $N_1 \approx 10^{16}\,\mathrm{cm^{-3}}$, and with $\eta_{10} = 0.8$, $\tau_1 = 100\,\mu$s, and $G_{01} = 1 \times 10^{22}\,\mathrm{cm^{-3}\,s^{-1}}$ for samples MD33 and MD42 we obtain $N_1 \approx 8 \times 10^{17}\,\mathrm{cm^{-3}}$. The slope of the $I^{\mathrm{PL}}(G)$ dependence at $G > G_{01}$ is closer to linear for samples MD33 and MD42 than for sample EM1256, which can be explained by a gradual decrease of τ_1 with increasing excitation intensity (Fig. 7). This may also affect the value of G_{01} (and N_1) obtained from SSPL. From the TRPL data [Fig. 16(b)], by taking $\eta_{10} = 0.8$, $\tau_{\mathrm{L}} = 1$ ns, and $G_{01} = 2.5 \times 10^{27}\,\mathrm{cm^{-3}\,s^{-1}}$, we obtain $N_1 \approx 2 \times 10^{18}\,\mathrm{cm^{-3}}$ for samples MD33 and MD42. By comparing these values with the SIMS data (Table I), we can see a rough agreement between N_1 and the concentration of carbon in these samples. On the other hand, the concentration of oxygen does not exceed $10^{17}\,\mathrm{cm^{-3}}$ in the studied GaN:C,Si samples, which gives an additional argument in favor of the $\mathrm{C_N}$ as the defect responsible for the YL1 band. Below, we present the results of first-principles calculations for the $\mathrm{C_N}$ defect.

B. Parameters of the $\mathrm{C_N}$ defect

The calculations were performed using the Heyd-Scuseria-Ernzerhof (HSE) hybrid functional [13]. The HSE functional was tuned to fulfill the generalized Koopmans condition for defects in GaN (fraction of exact exchange of 0.25, the range separation parameter of 0.161 $\mathrm{Å^{-1}}$) [42], in contrast to other theoretical approaches cited in Table III, where the HSE parameters are usually adjusted to yield the correct band gap. All calculations were performed in 300-atom hexagonal supercells at the Γ point, with plane-wave energy cutoffs of 500 eV. All atoms were relaxed within HSE to minimize forces to 0.05 eV/Å or less. Vertical transitions for neutral $\mathrm{C_N}$ (via $-/0$ level) were calculated using the neutral defect state eigenvalues with respect to the VBM, while those for charged $\mathrm{C_N^+}$ (via $0/+$ level) used the formation energy differences corrected for spurious electrostatic interactions following the Freysoldt, Neugebauer, and Van de Walle correction approach [43,44]. The ZPLs are computed by adding the defect relaxation energies to the PL maxima.

The experimentally found position of the PL band maximum ($\hbar\omega_{\max}$), the ZPL (E_0), and the defect ionization energy (E_A) for the YL1 and BL_C bands, compared with those calculated from first principles for the $\mathrm{C_N}$ defect in GaN, are tabulated in Table III. The agreement is relatively good for the ionization energies and ZPL of the PL bands. However, the calculated optical transition energies are consistently somewhat lower than the experimentally found PL band maxima.

The model parameters and transitions can be illustrated with a one-dimensional configuration coordinate diagram (Fig. 17). The vertical axis is the total energy of the defect system (atomic plus electron energy), and the horizontal axis

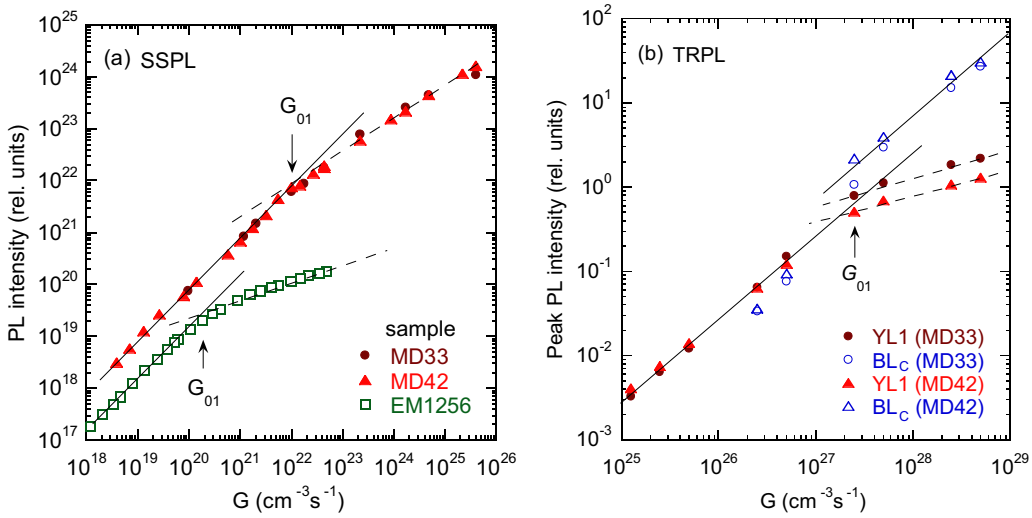

FIG. 16. Determination of the concentration of defects responsible for the YL1 band. (a) Intensity of the YL1 band from SSPL at 300 K. (b) Peak intensity of the YL1 and BL_C bands from TRPL at 300 K. The solid lines are linear dependences, and the dashed lines are the interpolation in the region of saturation of the YL1 band. The lines intersect at $G = G_{01}$ defined with Eq. (19) (SSPL) and Eq. (20) (TRPL).

is the generalized coordinate Q, which maps coordinates of all atoms to an effective one-dimensional coordinate. The ground state of the system is a parabola with a minimum at point a, which corresponds to the relaxed atomic structure of the C_N^- defect in n-type GaN prior to excitation.

Band-to-band excitations are represented by a vertical, dashed, upward arrow ending at point b. In the process, a free hole and a free electron are created, whereas the defect remains in the negatively charge state. The nonradiative capture of a free hole by the C_N^- defect results in a transition from point b to point c, with release of energy E_{A1} in a form of several phonons. The lattice around the C_N^0 defect relaxes, and the new equilibrium position is at point c. The system stays in this state for the PL lifetime $\tau_1 \approx 10\,\mu$s until a free electron is captured by the C_N^0 defect. The capture is radiative (downward arrow from point c to point d), observed as the YL1 band, and it is followed by lattice relaxation and emission of several phonons (transition from point d to point a).

With increasing excitation intensity, additional free electrons and holes are generated. The vertical upward arrow from point c to point e indicates excitation of an additional electron from the valence band to the conduction band in the vicinity of the C_N^0 defect. If the free hole is captured by the C_N^0 defect faster than the PL lifetime τ_{01}, the defect becomes C_N^+, and the lattice further relaxes from point e to point g with release of energy E_{A2} in the form of several phonons. The defect stays in this state for the PL lifetime $\tau_2 \approx 0.3$–1 ns until a free electron is captured by the C_N^+ defect. The capture is radiative (downward arrow from point g to point h), observed as the BL_C band, and it is followed by lattice relaxation and emission of several phonons (transition from point h to point c). From point c, the system may take a path c-d-a with emission of the YL1, or it repeats a cycle c-e-g-h-c with emission of the BL_C band if the excitation intensity is very high.

For a semi-insulating (formally p-type) GaN:C, where the Fermi level is close to the $-/0$ level of C_N, some of the C_N defects appear as the C_N^0 even in dark or at low excitation intensity (point c). These defects, after band-to-band excitation (transition c-e), may capture free holes (transition e-g) and cause the BL_C band (transition g-h) even at low excitation intensity. However, the capture of free holes by the C_N^0 defects is less efficient than the one by the C_N^- defects, so that the quantum efficiency of the YL1 band is higher than the efficiency of the BL_C band. Although the agreement between our calculations of optical transitions via C_N acceptor and experiment is satisfactory, our calculations also predict a barrier of 0.54 eV for nonradiative capture of a hole by the C_N^- (transition from point b to point c in Fig. 17). This is somewhat lower than the value of 0.73 eV obtained

TABLE III. Theoretical and experimental parameters of the C_N defect in GaN. All parameters are in eV.

	Transitions via $-/0$ level			Transitions via $0/+$ level			
	$\hbar\omega_{max}$ (YL1)	E_{01} (ZPL)	E_{A1}	$\hbar\omega_{max}$ (BL_C)	E_{02} (ZPL)	E_{A2}	Source
	2.14	2.60	0.90	2.70	3.15	0.35	[14,16]
	1.98	2.45	1.04	2.59	3.00	0.48	[17]
Theory	2.18	2.67	0.78		~3.05	~0.4	[49]
		2.56	0.89				[50]
	2.16	2.71	0.79			0.50	[48]
	2.08	2.57	0.93	2.73	3.14	0.36	This paper
Experiment	2.17 ± 0.02	2.587 ± 0.003	0.916 ± 0.003	2.85 ± 0.1	3.2 ± 0.1	0.3 ± 0.1	[6], This paper

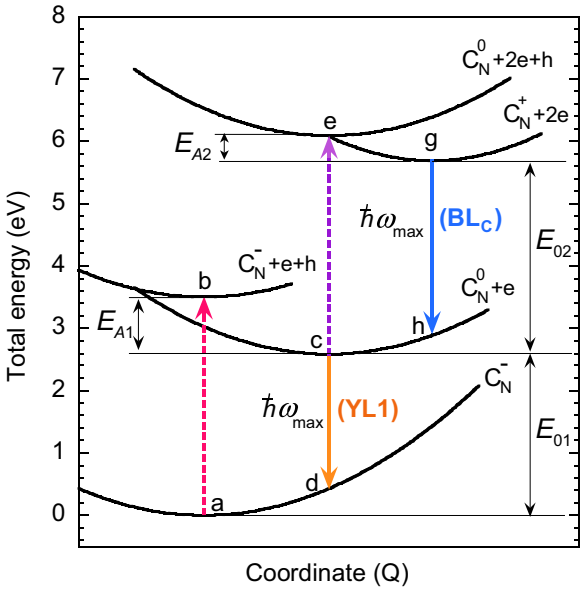

FIG. 17. Configuration coordinate diagram for the C_N defect in GaN. Parabola with a minimum at zero (point *a*) is the ground state of the system (C_N defect is filled with electrons: C_N^-). The transition *a*-*b* is the excitation of an electron from the valence band to the conduction band, with C_N remaining negatively charged. The transition *b*-*c* is the capture of a hole by the defect (the C_N^- becomes C_N^0). The transition *c*-*d* corresponds to the YL1 band maximum. The transition from *d* to *a* is the lattice relaxation after a photon is emitted. The transition from *c* to *a* causes the ZPL of the YL1 band with energy E_{01}. The parabola with the minimum at point *e* is identical to the parabola at *c*, but shifted upwards by $E_g = 3.503$ eV. The transition *e*-*g* corresponds to a capture of the second hole by the defect, which converts C_N^0 to C_N^+. The transition *g*-*h* corresponds to the maximum of the BL$_C$ band. The transition from *g* to *c* causes the ZPL of the BL$_C$ band with energy E_{02}.

in Ref. [45]. In a semiclassical model of nonradiative hole capture, this appears to predict a significant increase of the YL1 intensity with temperature. However, quantum tunneling lowers the effective barrier for hole capture by as much as ~0.5 eV [45], leading to a virtually temperature-independent hole-capture rate, which agrees with experiment.

We also would like to note that the measured BL$_C$ band electron-capture coefficient C_{nA} appears to be unusually large, while C_{pA} is unusually small. The deviation of these values from the values for other defects (Table II) can be explained to some extent by charges (acceptors are attractive centers for holes, while donors are attractive centers for electrons). However, the enhancement of the capture cross section due to Coulomb attraction of a carrier to a defect is expected to be by about a factor of 10 [45,46]. For the electron capture, the discrepancy could be due to a possible internal transition, as mentioned above. However, the unusually small value of the hole-capture coefficient remains an open question.

C. Identification of defect-related luminescence bands in undoped and C-doped GaN

We previously suggested that the YL band with a maximum at 2.2 eV in GaN is caused by the C_NO_N complexes, whereas a similar yellow band with a maximum at 2.1 eV is caused by isolated C_N defects [15,17]. The arguments for such attributions were that no secondary PL band could be found with increasing excitation intensity in MOVPE-grown GaN samples where the 2.2-eV band dominated, while the 2.1-eV band correlated in two HVPE-grown GaN samples with what appeared to be its secondary PL band with a maximum at 2.40 eV. In our new classification of PL bands in undoped GaN [33], this secondary PL band is indexed as the GL1 band ($\hbar\omega_{max} = 2.40$ eV), and the two yellow bands are indexed as the YL1 (2.20 eV) and YL3 (2.10 eV) bands. Since then, new experimental findings became available, including the results of this work, and we now revise the PL band attributions.

The YL1 band with the well-established fingerprints (Tables II and III) [6,32,33] is likely to be caused by optical transitions via the $-/0$ level of the C_N defect. This assignment agrees with the large hole-capture coefficient, the small electron-capture coefficient (in Table II these parameters are compared with parameters for the Mg_{Ga} and Zn_{Ga} acceptors responsible for the UVL and BL1 bands, respectively), and the dominance of this PL band in undoped GaN samples grown by MOVPE where the contamination with C is relatively high. Interestingly, recent studies by Iwinska *et al.* [47] demonstrate that doping of HVPE-grown GaN with carbon leads to *p*-type conductivity, which was measured with the Hall effect at temperatures between 625 and 1000 K. The activation energy of the acceptor is about 1.0 eV, and the YL band is the dominant feature in the PL spectrum from those samples.

The assignment of the YL1 band to the C_NO_N complex [15,48] is less likely since this complex is a deep donor, which is expected to capture holes less efficiently and electrons more efficiently than a deep acceptor. In addition, recent first-principles calculations predict that under thermal equilibrium at typical growth temperatures the concentration of isolated C_N defect should be higher than that of the defect complexes C_NSi_{Ga}, and the concentration of the C_NO_N complexes should be even lower [49]. The YL1 band is also unlikely to be caused by the C_NSi_{Ga} complex because only the YL1 band (one type of defect) is observed in undoped and Si-doped GaN grown by MOVPE [6]. Finally, the properties of the BL$_C$ band discovered in this work roughly match the properties of the sought-for secondary PL band of the C_N defect.

The BL$_C$ band is proposed to be caused by optical transitions via the $0/+$ level of the C_N defect (the secondary PL band). This assignment is consistent with a small hole-capture coefficient, large electron-capture coefficient, appearance of this band only at high excitation intensity in *n*-type GaN:C,Si, and appearance at low excitation intensity in semi-insulating GaN:C. Moreover, in a large set of *n*-type GaN samples, the BL$_C$ band correlates with the YL1 band (the $R\eta_2/\eta_1 = C_{pA2}N_{A2}/C_{pA1}N_{A1}$ ratio is about the same).

An alternative assignment could be that the BL$_C$ band is caused by a very deep donor other than C_N^+. One candidate is the C_NSi_{Ga} complex, for which we calculated the band maximum, ZPL, and ionization energy to be $\hbar\omega_{max} = 2.74$ eV, $E_0 = 3.21$ eV, and $E_A = 0.29$ eV, respectively. These parameters, which are also close to the results reported in Refs. [49,50], roughly match the experimentally found parameters of the BL$_C$ band (Table III). However, high intensity of the BL$_C$ band in semi-insulating GaN:C samples with

[Si] $\approx 10^{16}\,\mathrm{cm}^{-3}$ and relatively low intensity in conductive n-type GaN:C,Si samples with [Si] $\approx 10^{18}\,\mathrm{cm}^{-3}$ apparently contradict this assignment. In any case, the BL_C band should not be confused with the Zn_{Ga}-related BL1 band and C_NH_i-related BL2 band.

The BL2 band is attributed to the C_NH_i complex. We have established previously [22] that this PL band is a complex involving carbon and hydrogen; however, we could not reliably differentiate between the C_NH_i and $C_NO_NH_i$ defects. After careful analysis of the PL data from semi-insulating GaN samples (both undoped and C doped), we now conclude that the YL1 band emerges as a result of dissociation of the complex responsible for the BL2 band. Since the YL1 band is attributed to isolated C_N defect, then the BL2 band must be due to the C_NH_i. This assignment roughly agrees with first-principles calculations and is supported by the fact that the BL2 band appears only in semi-insulating GaN samples grown by MOVPE or HVPE where hydrogen is present in high concentrations [22]. The experimental data in this paper indicate that the C_NH_i defect has the $0/+$ state at 0.15 eV above the valence band and a hydrogenlike excited state very close to the conduction band. The BL2 band is caused by internal transitions from the excited state to the ground state of this donor.

We believe that Seager *et al.* [19,20] observed the BL2 band, not the BL_C band in semi-insulating GaN samples doped with C. They observed that the blue band bleached dramatically with time under UV exposure at low temperature, and it was quenched with increasing temperature above 130 K [20]. Moreover, in the experiments of Seager *et al.*, after pulsed excitation, the blue band decayed nearly exponentially at $T = 77$ K with the characteristic PL lifetime of about 0.3 μs (according to Fig. 6 in Ref. [20]), which is very similar to the BL2 band in our GaN:C samples.

The previously mentioned GL1 band behaves as a secondary PL band of some unknown defect [18]; however, it is unlikely to be related to carbon. Indeed, it was never observed in MOVPE-grown GaN where the concentration of carbon is significant. In contrast, it is often observed as the dominant defect-related PL band in HVPE-grown GaN where the concentration of carbon is relatively low and in some samples (such as sample RS280 in Refs. [17,18]) it is below the SIMS detection limit level of $5 \times 10^{15}\,\mathrm{cm}^{-3}$. After careful analysis of PL from many HVPE-grown GaN samples, we conclude that there is no correlation between the GL1 and YL1 bands, as well as between the GL1 and YL3 bands. The apparent correlation between the GL1 and YL3 bands for two samples reported in Ref. [17] was accidental. The origin of the GL1 band in HVPE-grown GaN samples remains a puzzle.

The YL3 band with a maximum at 2.10 eV and the ZPL at 2.36 eV is a very special PL band, which is observed only in HVPE-grown GaN. It is not related to the GL1 band, but apparently related to the RL3 band with a maximum at 1.8 eV [51]. Further investigations are under way to determine the properties of the YL3 and RL3 bands and their mutual relation and the defect identity.

Finally, we address the question whether the V_{Ga} (isolated or complexed with impurities) may be responsible for the YL band in GaN. From a large amount of experimental and theoretical data, we conclude that the V_{Ga}-related defects are either nonradiative or very inefficient hole traps in GaN and thus do not contribute to the experimentally observed YL band. Indeed, the lifetime of the YL is always long (in microsecond range), and if this band was caused by the radiative capture of free holes by the $3-/2-$ level of the V_{Ga} located at 2.8 eV above the valence band [52] its intensity would be extremely weak, because this slow radiative capture of minority carriers (holes) cannot compete with very fast nonradiative capture of holes by the C_N, Zn_{Ga}, Mg_{Ga}, and unknown nonradiative defects and with fast formation of excitons.

Although in early experiments with positron annihilation an apparent correlation between the concentration of V_{Ga} and the yellow band intensity was noted [11], further experiments were unable to confidently confirm this correlation [5], and even anticorrelation between the YL band intensity and the V_{Ga} concentration has been reported [53]. Recently, we studied HVPE-grown GaN samples with PL and positron annihilation spectroscopy (PAS) [32]. The concentration of the V_{Ga} from PAS measurements was estimated as 6×10^{17} and $1 \times 10^{17}\,\mathrm{cm}^{-3}$ for samples H3 and H202, respectively. However, the concentration of the defect responsible for the YL band was only 2.4×10^{14} and $8 \times 10^{14}\,\mathrm{cm}^{-3}$ in these samples, respectively. Other radiative defects in sample H3 had even lower concentrations. Although first-principles calculations predict that several V_{Ga}-related defects could cause luminescence bands similar to the YL1 band in GaN [52], a more detailed analysis shows that at least some of them (e.g., the $V_{Ga}O_N$ complex) could be centers of efficient nonradiative recombination [54]. It should be emphasized that we were unable to detect any YL band, other than the YL1 and YL3 bands, in a very large set of GaN samples grown by different techniques. Thus, if any V_{Ga}-related defect causes a PL band with position close to the YL1 and YL3 bands, its intensity should be much weaker.

V. CONCLUSION

We observed a PL band with unusual properties in MOVPE-grown GaN samples doped with carbon or codoped with carbon and silicon. This is the BL_C band with a maximum at 2.9 eV, which has a characteristic lifetime of about 1 ns, independent of temperature and inversely proportional to the concentration of free electrons in n-type GaN samples. This blue band should not be confused with the Zn-related BL1 band (the maximum at 2.9 eV) and with the C_NH_i-related BL2 band (the maximum at 3.0 eV). As compared to dominant radiative acceptors in n-type GaN, the hole-capture coefficient for the BL_C-related defect is very small ($\sim 10^{-10}\,\mathrm{cm}^3/\mathrm{s}$), and its apparent electron-capture coefficient is extremely large ($\sim 10^{-9}\,\mathrm{cm}^3/\mathrm{s}$), which explains very low quantum efficiency of this PL band and the fact that it was not previously detected. We attribute the YL1 and BL_C bands to electron transitions via the $-/0$ and $0/+$ transitional levels, respectively, of the C_N defect. The characteristic parameters of these PL bands agree with first-principles calculations.

ACKNOWLEDGMENTS

The work was supported by the NSF (Grant No. DMR-1410125) and the Virginia Commonwealth University Center for High Performance Computing.

[1] M. A. Reshchikov and H. Morkoç, J. Appl. Phys. **97**, 061301 (2005).

[2] T. Ogino and M. Aoki, Jpn. J. Appl. Phys. **19**, 2395 (1980).

[3] O. Kucheyev, M. Toth, M. R. Phillips, J. S. Williams, C. Jagadish, and G. Li, J. Appl. Phys. **91**, 5867 (2002).

[4] R. Armitage, W. Hong, Q. Yang, H. Feick, J. Gebauer, E. R. Weber, S. Hautakangas, and K. Saarinen, Appl. Phys. Lett. **82**, 3457 (2003).

[5] F. Reurings and F. Tuomisto, Interplay of Ga vacancies, C impurities and yellow luminescence in GaN, in *Gallium Nitride Materials and Devices II*, edited by H. Morkoç and C. W. Litton, Proceedings of SPIE Vol. 6473 (SPIE, Bellingham, WA, 2007), p. 64730M.

[6] M. A. Reshchikov, J. D. McNamara, F. Zhang, M. Monavarian, A. Usikov, H. Helava, Yu. Makarov, and H. Morkoç, Phys. Rev. B **94**, 035201 (2016).

[7] M. A. Reshchikov, N. M. Albarakati, M. Monavarian, V. Avrutin, and H. Morkoc, J. Appl. Phys. **123**, 161520 (2018).

[8] J. Neugebauer and C. G. Van de Walle, Appl. Phys. Lett. **69**, 503 (1996).

[9] T. Mattila and R. M. Nieminen, Phys. Rev. B **55**, 9571 (1997).

[10] This attribution partially agreed with the proposal of Ogino and Aoki that the acceptor of the YL band is a complex involving a carbon atom and the gallium vacancy.

[11] K. Saarinen, T. Laine, S. Kuisma, J. Nissilä, P. Hautojärvi, L. Dobrzynski, J. M. Baranowski, K. Pakula, R. Stepniewski, M. Wojdak, A. Wysmolek, T. Suski, M. Leszczynski, I. Grzegory, and S. Porowski, Phys. Rev. Lett. **79**, 3030 (1997).

[12] R. Zhang and T. F. Kuech, Appl. Phys. Lett. **72**, 1611 (1998).

[13] J. Heyd, G. E. Scuseria, and M. Ernzerhof, J. Chem. Phys. **118**, 8207 (2003).

[14] J. L. Lyons, A. Janotti, and C. G. Van de Walle, Appl. Phys. Lett. **97**, 152108 (2010)

[15] D. O. Demchenko, I. C. Diallo, and M. A. Reshchikov, Phys. Rev. Lett. **110**, 087404 (2013).

[16] J. L. Lyons, A. Janotti, and C. G. Van de Walle, Phys. Rev. B **89**, 035204 (2014).

[17] M. A. Reshchikov, D. O. Demchenko, A. Usikov, H. Helava, and Yu. Makarov, Phys. Rev. B, **90**, 235203 (2014).

[18] M. A. Reshchikov, J. D. McNamara, A. Usikov, H. Helava, and Yu. Makarov, Phys. Rev. B **93**, 081202(R) (2016).

[19] C. H. Seager, A. F. Wright, J. Yu, and W. Götz, J. Appl. Phys. **92**, 6553 (2002).

[20] C. H. Seager, D. R. Tallant, J. Yu, and W. Götz, J. Lumin. **106**, 115 (2004).

[21] D. O. Demchenko and M. A. Reshchikov, Phys. Rev. B **88**, 115204 (2013).

[22] D. O. Demchenko, I. C. Diallo, and M. A. Reshchikov, J. Appl. Phys. **119**, 035702 (2016).

[23] A. Lesnik, M. P. Hoffmann, A. Fariza, J. Bläsing, H. Witte, P. Veit, F. Hörich, C. Berger, J. Hennig, A. Dadgar, and A. Strittmatter, Phys. Status Solidi B **254**, 1600708 (2016).

[24] The SIMS data for sample EM1256 were provided by S.-P. Guo and D. W. Gotthold (EMCORE).

[25] I. Pelant and J. Valenta, *Luminescence Spectroscopy of Semiconductors* (Oxford University, Oxford, 2012), p. 61.

[26] M. A. Reshchikov, A. A. Kvasov, M. F. Bishop, T. McMullen, A. Usikov, V. Soukhoveev, and V. A. Dmitriev, Phys. Rev. B **84**, 075212 (2011).

[27] M. A. Reshchikov, M. A. Foussekis, J. D. McNamara, A. Behrends, A. Bakin, and A. Waag, J. Appl. Phys. **111**, 073106 (2012).

[28] M. A. Reshchikov, D. O. Demchenko, J. D. McNamara, S. Fernández-Garrido, and R. Calarco, Phys. Rev. B **90**, 035207 (2014).

[29] D. G. Thomas, J. J. Hopfield, and W. M. Augustyniak, Phys. Rev. **140**, A202 (1965).

[30] A. P. Levanyuk and V. V. Osipov, Sov. Phys. Usp. **24**, 187 (1981).

[31] M. A. Reshchikov, Internal quantum efficiency of photoluminescence in wide-bandgap semiconductors, in *Photoluminescence: Applications, Types and Efficacy*, edited by M. A. Case and B. C. Stout (Nova Science, New York, 2012), pp. 53–120.

[32] M. A. Reshchikov, A. Usikov, H. Helava, Yu. Makarov, V. Prozheeva, I. Makkonen, F. Tuomisto, J. H. Leach, and K. Udwary, Sci. Rep. **7**, 9297 (2017).

[33] M. A. Reshchikov, J. D. McNamara, M. Toporkov, V. Avrutin, H. Morkoç, A. Usikov, H. Helava, and Yu. Makarov, Sci. Rep. **6**, 37511 (2016).

[34] M. A. Reshchikov, J. D. McNamara, A. Usikov, H. Helava, and Yu. Makarov, Mater. Res. Soc. Proc. **1736**, T05 (2015).

[35] M. A. Reshchikov, H. Morkoç, S. S. Park, and K. Y. Lee, Appl. Phys. Lett. **81**, 4970 (2002).

[36] R. Y. Korotkov, M. A. Reshchikov, and B. W. Wessels, Physica B **325**, 1 (2003).

[37] M. A. Reshchikov, J. Appl. Phys. **115**, 103503 (2014).

[38] G. Davies, Optical measurements of point defects, in *Identification of Defects in Semiconductors*, edited by M. Stavola, Semiconductors and Semimetals Vol. 51, Part B (Academic Press, San Diego, CA, 1999), pp. 1–92.

[39] M. F. Thomaz and G. Davies, Proc. R. Soc. A **362**, 405 (1978).

[40] M. A. Reshchikov, Y. T. Moon, X. Gu, B. Nemeth, J. Nause, and H. Morkoç, Physica B **376–377**, 715 (2006).

[41] The obtained value of $\tau_3 = 45$ ns in the range 10–60 ns is lower than the value found for the BL2 band in experiments with another setup (200–400 ns), because the BL2 decay is not purely exponential.

[42] D. O. Demchenko, I. C. Diallo, and M. A. Reshchikov, Phys. Rev. B **97**, 205205 (2018).

[43] C. Freysoldt, J. Neugebauer, and C. G. Van de Walle, Phys. Rev. Lett. **102**, 016402 (2009).

[44] C. Freysoldt, J. Neugebauer, and C. G. Van de Walle, Phys. Status Solidi B **248**, 1067 (2010).

[45] A. Alkauskas, Q. Yan, and C. G. Van de Walle, Phys. Rev. B **90**, 075202 (2014).

[46] M. A. Reshchikov and R. Y. Korotkov, Phys. Rev. B **64**, 115205 (2001).

[47] M. Iwinska, R. Piotrzkowski, E. Litwin-Staszewska, T. Sochacki, M. Amilusik, M. Fijalkowski, B. Lucznik, and M. Bockowski, Appl. Phys. Express **10**, 011003 (2017).

[48] H. S. Zhang, L. Shi, X.-B. Yang, Y.-J. Zhao, K. Xu, and L.-W. Wang, Adv. Opt. Mater. **5**, 1700404 (2017).

[49] S. G. Christenson, W. Xie, Y. Y. Sun, and S. B. Zhang, J. Appl. Phys. **118**, 135708 (2015).

[50] M. Matsubara and E. Bellotti, J. Appl. Phys. **121**, 195702 (2017).

[51] M. A. Reshchikov, J. D. McNamara, A. Usikov, H. Helava, and Yu. Makarov, Sci. Rep. **8**, 8091 (2018).

[52] J. L. Lyons, A. Alkauskas, A. Janotti, and C. G. Van de Walle, Phys. Status Solidi B **252**, 900 (2015).

[53] M. Huber, M. Silvestri, L. Knuuttila, G. Pozzovivo, A. Andreev, A. Kadashchuk, A. Bonanni, and A. Lundskog, Appl. Phys. Lett. **107**, 032106 (2015).

[54] A. Alkauskas, C. E. Dreyer, J. L. Lyons, and C. G. Van de Walle, Phys. Rev. B **93**, 201304(R) (2016).